Sterol Regulatory Element Binding Protein 2 Activation of NLRP3 Inflammasome in Endothelium Mediates Hemodynamic-Induced Atherosclerosis Susceptibility

Han Xiao, Min Lu, Ting Yang Lin, Zhen Chen, Gang Chen, Wei-Chi Wang, Traci Marin, Tzu-pin Shentu, Liang Wen, Brendan Gongol, Wei Sun, Xiao Liang, Ju Chen, Hsien-Da Huang, Joao H.F. Pedra, David A. Johnson and John Y-J. Shyy

Circulation. 2013;128:632-642; originally published online July 9, 2013;
doi: 10.1161/CIRCULATIONAHA.113.002714
Circulation is published by the American Heart Association, 7272 Greenville Avenue, Dallas, TX 75231

Print ISSN: 0009-7322. Online ISSN: 1524-4539

Sterol Regulatory Element Binding Protein 2 Activation of NLRP3 Inflammasome in Endothelium Mediates Hemodynamic-Induced Atherosclerosis Susceptibility

Han Xiao, MD, PhD; Min Lu, MD, PhD; Ting Yang Lin, MS; Zhen Chen, PhD; Gang Chen, MD; Wei-Chi Wang, PhD; Traci Marin, MS; Tzu-pin Shentu, PhD; Liang Wen, PhD; Brendan Gongol, MS; Wei Sun, MD; Xiao Liang, MD, PhD; Ju Chen, PhD; Hsien-Da Huang, PhD; Joao H.F. Pedra, PhD; David A. Johnson, PhD; John Y-J. Shyy, PhD

Background—The molecular basis for the focal nature of atherosclerotic lesions is poorly understood. Here, we explored whether disturbed flow patterns activate an innate immune response to form the NLRP3 inflammasome scaffold in vascular endothelial cells via sterol regulatory element binding protein 2 (SREBP2).

Methods and Results—Oscillatory flow activates SREBP2 and induces NLRP3 inflammasome in endothelial cells. The underlying mechanisms involve SREBP2 transactivating NADPH oxidase 2 and NLRP3. Consistently, SREBP2, NADPH oxidase 2, and NLRP3 levels were elevated in atheroprone areas of mouse aortas, suggesting that the SREBP2-activated NLRP3 inflammasome causes functionally disturbed endothelium with increased inflammation. Mimicking the effect of atheroprone flow, endothelial cell–specific overexpression of the activated form of SREBP2 synergized with hyperlipidemia to increase atherosclerosis in the atheroresistant areas of mouse aortas.

Conclusions—Atheroprone flow induces NLRP3 inflammasome in endothelium through SREBP2 activation. This increased innate immunity in endothelium synergizes with hyperlipidemia to cause topographical distribution of atherosclerotic lesions. **(*Circulation*. 2013;128:632-642.)**

Key Words: atherosclerosis ■ endothelial cell ■ NLRP3 protein, human ■ shear stress ■ sterol regulatory element binding proteins

Atherosclerosis preferentially develops at branches and curvatures in the arterial tree. Cardiovascular risk factors such as hyperlipidemia, smoking, and hypertension increase the prevalence and severity of lesions in these atheroprone regions.[1] At the cellular and molecular levels, disturbed flow patterns with low shear stress such as those found at vascular branches and curvatures increase the expression of genes such as interleukin 1β (IL-1β) and NADPH oxidase (NOX) to promote inflammatory and oxidative stresses in vascular endothelial cells (ECs).[2,3] Such hemodynamic-induced functionally disturbed endothelium predisposes localized areas to become atherogenic, with ensuing monocyte recruitment and foam cell formation. Although extensive studies have revealed EC gene expression profiles associated with the atheroprone flow patterns, the key molecular events linking mechanical stimuli to atherogenic responses remain undetermined.

Editorial see p 579
Clinical Perspective on p 642

Sterol regulatory element binding (SRE) protein 2 (SREBP2) plays a canonical role in cholesterol homeostasis by its transcriptional regulation of molecules involved in cholesterol biosynthesis and low-density lipoprotein (LDL) uptake.[4] Cholesterol depletion leads to increased expression of SREBP2, along with its intronic microRNA-33 (miR-33), which replenishes cellular cholesterol by inducing genes that encode proteins such as HMG-CoA reductase and LDL receptor and suppressing the ATP-binding cassette transporter 1 (ABCA1).[5,6] Conversely, elevated levels of sterols suppress SREBP expression, thereby lowering cellular cholesterol levels. This homeostasis might be disrupted by atheroprone flow patterns, which induce sustained activation of SREBP1 and perturbation of EC function.[7]

Received November 8, 2012; accepted June 6, 2013.

From the Division of Biomedical Sciences (H.X., T.Y.L., Z.C., T.M., T.-p.S., L.W., B.G., W.S., D.A.J., J.Y.-J.S.) and Center for Disease Vector Research and Department of Entomology (G.C., J.H.F.P.), University of California, Riverside; Institute of Vascular Medicine of Peking University Third Hospital, Beijing, China (H.X.); Department of Medicine, University of California, San Diego, La Jolla (M.L., Z.C., J.C., J.Y.-J.S.); Department of Biological Science and Technology, Institute of Bioinformatics and Systems Biology, National Chiao Tung University, HsinChu, Taiwan (W.-C.W., H.-D.H.); and Cardiovascular Research Center, Medical School, Xi'an Jiaotong University, Xi'an, China (X.L., J.Y.-J.S.).

The online-only Data Supplement is available with this article at http://circ.ahajournals.org/lookup/suppl/doi:10.1161/CIRCULATIONAHA.113.002714/-/DC1.

Correspondence to John Y-J. Shyy, PhD, Department of Medicine/Division of Cardiology, University of California, San Diego, 9500 Gilman Dr, La Jolla, CA 92093. E-mail jshyy@ucsd.edu

The connection between hemodynamic-induced endothelial dysfunction and inflammatory and oxidative stresses is poorly understood. However, aberrant lipid metabolism, unbalanced redox states, and innate immunity in phagocytes are linked through NLRP3 inflammasome with subsequent cleavage and activation of interleukin (IL)-1 family proteins.[8] Moreover, cholesterol crystals activate the NLRP3 inflammasome and increase the secretion of mature IL-1β in monocyte/macrophages.[9,10] LDL receptor–deficient mice receiving bone marrow–derived cells lacking NLRP3, ASC, or IL-1α/β were resistant to the development of diet-induced atherosclerosis.[9] Alone, systemic activation of NLRP3 inflammasome in macrophages does not explain the preferential localization of atherosclerosis in the arterial tree.

Disturbed flow can activate NOX and induce reactive oxygen species (ROS).[11] This raises the possibility that inflammasome is involved in oxidative stress in ECs. Additionally, a recent report of minute cholesterol crystals appearing early in atherosclerotic lesions[9] suggests a linkage between hemodynamic stimuli, SREBP2 activation, and NLRP3 inflammasome in ECs, all linked to atherosclerosis. Using in vitro and in vivo approaches, we report here that the atheroprone flow–induced endothelial inflammation and oxidative stress are mediated through SREBP2-elicited NLRP3 inflammasome. Our findings reinforce a primary role of EC innate immunity in the origin of atherosclerosis.

Methods

Antibodies and Reagents

Anti-SREBP2 antibody was from BD Transduction Laboratory and Abcam; anti–IL-1β, anti-caspase-1, and anti–α-tubulin, horseradish peroxide–conjugated anti-rabbit and anti-mouse antibodies were from Cell Signaling Technology; anti-ABCG1, anti-NLRP3, anti-NOX2 antibodies were from Abcam; anti-ABCA1 antibody was from Millipore; and anti-ASC antibody was from Enzo Life Science. The caspase-1 inhibitor Z-YVAD-FMK was from Biovision. 25-Hydroxycholesterol (25-HC) and methyl-β-cyclodextrin were from Sigma.

Cell Culture

Human umbilical vein ECs (HUVECs) were cultured in medium M199 (Gibco) supplemented with 15% FBS (Omega), 3 ng/mL β-EC growth factor, 4 U/mL heparin, and 100 U/mL penicillin-streptomycin. Total cholesterol was measured with the Infinity Total Cholesterol Kit (Thermo Scientific). Caspase-1 activity was measured with the use of the Caspase-1/ICE Colorimetric Assay Kit (R&D Systems). Primary mouse lung ECs were isolated as described.[12]

Shear Stress Experiments

A circulating flow system was used to impose shear stress on confluent monolayers of cells seeded on glass slides as described.[13] A reciprocating syringe pump connected to the circulating system introduced a sinusoidal (1 Hz) component onto the shear stress. The atheroprotective pulsatile shear flow (PS) or atheroprone oscillatory shear flow (OS) generated shear stresses of 12±4 or 1±4 dynes/cm^2, respectively. The flow system was enclosed in a chamber held at 37°C and ventilated with 95% humidified air plus 5% CO_2.

siRNA Knockdown

HUVECs at 50% to 70% confluence were transfected with SREBP2 siRNA, NLRP3 siRNA, ASC siRNA, NOX2 siRNA, or control siRNA at 20 nmol/L with Lipofectamine 2000 RNAi Max (Invitrogen). Experiments were performed with these cells at 48 hours after transfection.

Adenovirus Construction and Infection

Recombinant adenovirus encoding the mature form of SREBP2, that is, Ad-HA-SREBP2(N), was created, amplified, and titrated as reported previously.[14] For adenovirus infection, the virus mixture was added to 70% confluent cultured HUVECs and incubated for 12 hours. Adenovirus (Ad)-null was an infection control. The infected cells were then incubated in fresh growth medium for 24 hours before RNA or protein extraction.

Binding Site Prediction

The potential SREBP2 binding sites on selected human and mouse genes were predicted by use of the position weight matrix algorithm from TRANSFAC[15] to scan the promoter regions of the genes. The promoter regions were defined as −3000 to 500 from the transcriptional start site of the gene.

Chromatin Immunoprecipitation Assay

Chromatin immunoprecipitation assays were performed with standard protocols[16] using antibodies for SREBP2 (BD Transduction Laboratory) and mouse IgG (Cell Signaling).

EC-SREBP2(N) Transgenic Mice

Animal experimental protocols were approved by the Institutional Animal Care and Use Committee of the University of California, Riverside. The creation of the EC-SREBP2(N)-Tg mouse model is described in the online-only Data Supplement. Littermates carrying ApoE$^{-/-}$ or EC-SREBP2(N)$^{+/+}$ApoE$^{-/-}$ genotypes were generated by crossing EC-SREBP2(N)-Tg mice and ApoE$^{-/-}$ mice. All mice were housed in colony cages with a 14-hour light/10-hour dark cycle and fed Rodent Diet 5001 (PMI Nutrition International) ad libitum unless otherwise indicated. Eight-week-old male EC-SREBP2(N)$^{+/+}$ApoE$^{-/-}$ mice and their male EC-SREBP2(N)$^{-/-}$ApoE$^{-/-}$ littermates were fed a high-fat, high-cholesterol diet containing 15% fat, 1.25% cholesterol, and 0.5% sodium cholate (Harlan Teklad) ad libitum. Eight weeks after the diet treatment, all mice were euthanized. In addition, 24-week-old male EC-SREBP2(N)$^{+/+}$ApoE$^{-/-}$ mice and their male EC-SREBP2(N)$^{-/-}$ApoE$^{-/-}$ littermates were fed normal chow. Mouse aortas were isolated to assess the extent and distribution of lesions by Oil Red O staining.[17] Lesion area was measured with Image Pro Plus 6.0 (Media Cybernetics) and expressed as a percentage of the total area of aorta. Plasma levels of total cholesterol, high-density lipoprotein cholesterol, and triglycerides were determined with assay kits from Wako Pure Chemicals (Tokyo, Japan).

Statistical Analysis

Data are expressed as mean±SEM (n=3 unless otherwise noted). In parametric data, the Student *t* test or ANOVA was used to analyze the differences among groups if data were determined to be normally distributed. For nonparametric data, the Mann-Whitney *U* test with the exact method was used to analyze differences between 2 groups. Values of $P<0.05$ were considered statistically significant.

Results

Coinduction of SREBP2 and miR-33 in ECs by OS

Initially, we examined the effects of PS and OS on the expression of SREBP2 in ECs. Imposition of OS, but not PS, activated SREBP2, as evidenced by the increased level of the mature form of SREBP2, namely SREBP2(N), and SREBP2 mRNA (Figure 1A and 1B). Given that miR-33 is intronic with SREBP-2, OS also elevated the level of miR-33 (Figure 1B). Additionally, the expression of SREBP2-targeted genes, that is, HMG-CoA reductase, HMG-CoA synthase, squalene synthase, and LDL receptor, was higher with OS

than PS (Figure 1C). The miR-33–targeted ABCA1, but not ABCG1, was downregulated at both the transcriptional and translational levels (Figure 1D and 1E). Thus, OS increased the expression of genes involved in cholesterol synthesis and uptake while decreasing ABCA1, which is involved in cholesterol efflux. In line with these changes, the cholesterol content of HUVECs was greater with OS than PS (Figure 1F). One possible mechanism for OS induction of SREBP2 is that the action of OS is secondary to sterol depletion. Consequently, we examined whether sterol replenishment with 25-HC blocks the effect of OS on SREBP2 activation. Although 25-HC and methyl-β-cyclodextrin reduced and increased SREBP activation in HUVECs, respectively, incubation of 25-HC had little effect on OS-induced SREBP2 expression (Figure 1G). Interestingly, overexpression of the mature form of SREBP2, that is, SREBP2(N) or premiR33, increased the cholesterol content (Figure IA and IB in the online-only Data Supplement. However, siRNA knockdown of SREBP2, but not miR-33, abolished OS-induced cholesterol accumulation (Figure IC and ID in the online-only Data Supplement). Consequently, we focused on the role of SREBP2 in OS-disturbed endothelial functions.

OS Induces NLRP3 Inflammasome in ECs via SREBP2

The atheroprone nature of OS is due largely to its imposition of inflammatory and oxidative stresses on ECs.[18] Because SREBP1a induces caspase-1–activated NLRP3 inflammasome in macrophages, resulting in cleavage and secretion of IL-1 family cytokines,[19] we investigated whether OS induces inflammasome in ECs. The levels of cleaved caspase-1 and IL-1β were greater in ECs with OS than PS (Figure 2A). Because OS induced SREBP2 maturation, we explored whether SREBP2(N) overexpression mimics OS to induce inflammasome in ECs. As expected, increased cleavage of caspase-1 and IL-1β was found in ECs infected with Ad-SREBP2(N) encoding SREBP2(N) (Figure 2B). Consistent with this finding, ectopic expression of SREBP2(N) increased caspase-1 activity in ECs (Figure 2C). With siRNA knockdown of endogenous SREBP2, OS-induced cleavage of caspase-1 or IL-1β was reduced (Figure 2D). Similar results were found when the inflammasome components NLRP3 and ASC were knocked down (Figure 2E and 2F). Together, these results suggest that SREBP2 mediates OS-induced NLRP3 inflammasome in ECs.

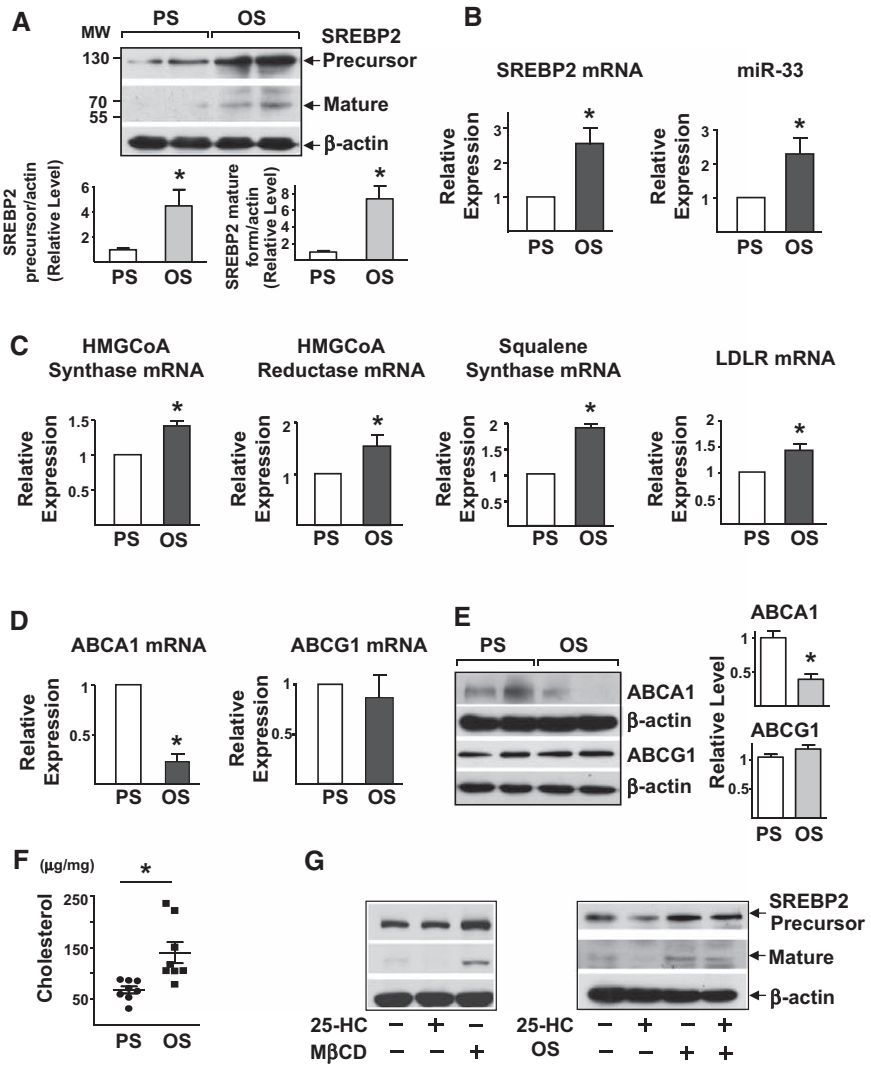

Figure 1. Oscillatory shear flow (OS) induces sterol regulatory element binding protein 2 (SREBP2) and miR-33 in human umbilical vein endothelial cells (HUVECs). HUVECs were exposed to a pulsatile shear flow (PS; 12±4 dynes/cm^2) or OS (1±4 dynes/cm^2) for 14 hours. **A**, Representative immunoblot for precursor SREBP2 and mature form of SREBP2. **B**, Analysis of levels of SREBP2 mRNA and miR-33 by quantitative real-time–polymerase chain reaction. **C**, The mRNA levels of HMG-CoA synthase, HMG-CoA reductase, squalene synthase, and low-density lipoprotein receptor (LDLR). **D**, mRNA levels of ATP-binding cassette transporter (ABC) A1 and ABCG1. **E**, Representative immunoblot for ABCA1 and ABCG1. **F**, Total cellular cholesterol level (n=8). **G**, Representative immunoblot for precursor SREBP2 and mature form of SREBP2 in HUVECs treated with methyl-β-cyclodextrin (MβCD), 25-hydroxycholesterol (25-HC; 1 μg/mL), or OS plus 25-HC (1 μg/mL). Data are mean±SEM from at least 3 independent experiments. The Student *t* test or Mann-Whitney *U* test with the exact method was used. MW indicates molecular weight. *P<0.05.

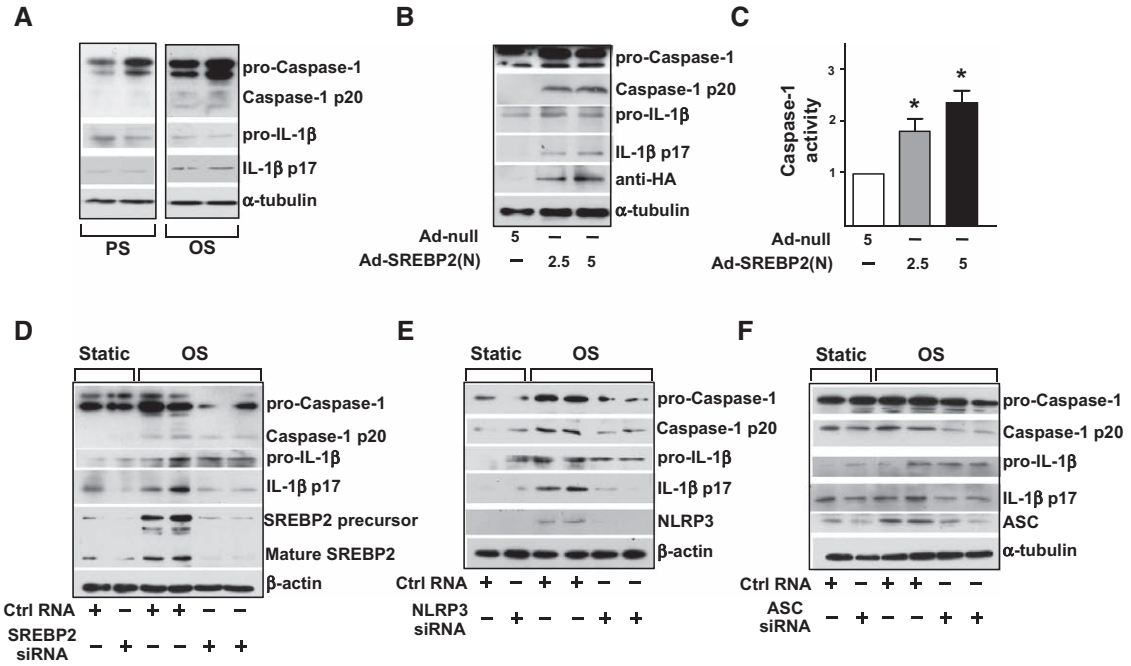

Figure 2. Oscillatory shear flow (OS) induces NLRP3 inflammasomes in endothelial cells (ECs) via sterol regulatory element binding protein 2 (SREBP2). **A**, Representative immunoblot for procaspase-1, caspase-1 p20, pro–interleukin (IL)-1β, and IL-1β p17 in human umbilical vein ECs (HUVECs) exposed to pulsatile shear flow (PS) or OS for 14 hours and (**B**) in HUVECs treated with adenovirus-null (Ad-null; 5 multiplicities of infection [MOI]) or adenovirus-SREBP2(N) tagged with HA [Ad-SREBP2(N), 2.5 or 5 MOI]. **C**, Caspase-1 activity of extracts from HUVECs treated with Ad-null 5 MOI or Ad-SREBP2(N) 2.5 or 5 MOI. Data are mean±SEM normalized to the Ad-null group for each independent experiment. The Mann-Whitney *U* test with the exact method was used. **P*<0.05 vs Ad-null. **D**, Representative immunoblot of procaspase-1, caspase-1 p20, pro-IL-1β, IL-1β p17, SREBP2 precursor, and mature form of SREBP2 in HUVECs transfected with 20 nmol/L control RNA or SREBP2 siRNA for 48 hours and then exposed to static conditions or OS for 14 hours. **E**, Representative immunoblot for procaspase-1, caspase-1 p20, pro-IL-1β, IL-1β p17, and NLPR3 in HUVECs transfected with 20 nmol/L control RNA or NLRP3 siRNA for 48 hours and then exposed to static conditions or OS for 14 hours. **F**, Representative immunoblot of procaspase-1, caspase-1 p20, pro-IL-1β, IL-1β p17, and ASC in HUVECs transfected with 20 nmol/L control RNA or ASC siRNA for 48 hours and then exposed to static conditions or OS for 14 hours.

SREBP2 Upregulates NOX2 With Increased ROS Production

We then investigated the underlying mechanism by which SREBP2 regulates the OS-induced inflammasome in ECs. The ROS level is increased by NLRP3 activators such as asbestos and silica,[20] and increased ROS are secondary messengers essential for inducing NLRP3 inflammasome.[20,21] Given that OS is known to increase ROS production,[22] we examined SREBP2 augmentation in relation to ROS production. The intracellular level of ROS increased in ECs infected with Ad-SREBP2(N) encoding the mature form of SREBP2 (Figure 3A). To assess the source of the increased level of ROS in ECs overexpressing SREBP2(N), we monitored ROS-generating mitochondria using MitoSOX, a selective mitochondrial superoxide indicator. Rotenone, the complex I inhibitor, greatly increased mitochondrial ROS production, but Ad-SREBP2(N) overexpression was without effect (Figure 3B). Therefore, the increased ROS production caused by SREBP2 activation probably did not originate from mitochondria. Bioinformatics predicted the presence of 3 SREs in the promoter region of the human *NOX2* gene (−2381/−2367, −867/−861, and −674/668 bp; Figure 3C). Consistent with this prediction, the levels of NOX2 mRNA and protein increased in Ad-SREBP2(N)–infected HUVECs and in ECs isolated from transgenic mice overexpressing SREBP2(N) in endothelium [EC-SREBP2(N)-Tg] (Figure 3D–3F). Of note, the levels of other NADPH oxidase subunits (except NOX1) were not significantly increased in these cells (Figure II in the online-only Data Supplement). Chromatin immunoprecipitation assay demonstrated an increase in the binding of SREBP2 to the 3 SREs containing the consensus sequence of CACC(T)CCA (Figure 3G). To investigate whether SREBP2 is required for OS-induced NOX2, we knocked down SREBP2 and found that the OS-induced NOX2 was partially suppressed (Figure 3H). Furthermore, NOX2 knockdown inhibited the OS-induced caspase-1 and IL-1β cleavage (Figure 3I). A similar inhibitory effect was found in NOX2$^{-/-}$ mouse embryonic fibroblasts (Figure III in the online-only Data Supplement). These results suggest that the SREBP2-transactivated NOX2 is required for OS-induced inflammasome in ECs.

SREBP2 Upregulates NLRP3 Expression

Bioinformatics also predicted the presence of an SRE located at −1379/−1368 bp in the promoter region of the *NLRP3* gene (Figure 4A). As expected, NLRP3 expression was increased in Ad-SREBP2(N)–infected HUVECs (Figure 4B and 4C) and ECs isolated from EC-SREBP2(N)-Tg mice (Figure 4D). Chromatin immunoprecipitation assays demonstrated an increase in the binding of SREBP2 to SRE containing the consensus sequence CCGCCACCACAC (Figure 4E). To investigate whether SREBP2 is required for OS-induced NLRP3 expression, we knocked down SREBP2. Accordingly, the level of NLRP3 responding to OS was decreased (Figure 4F).

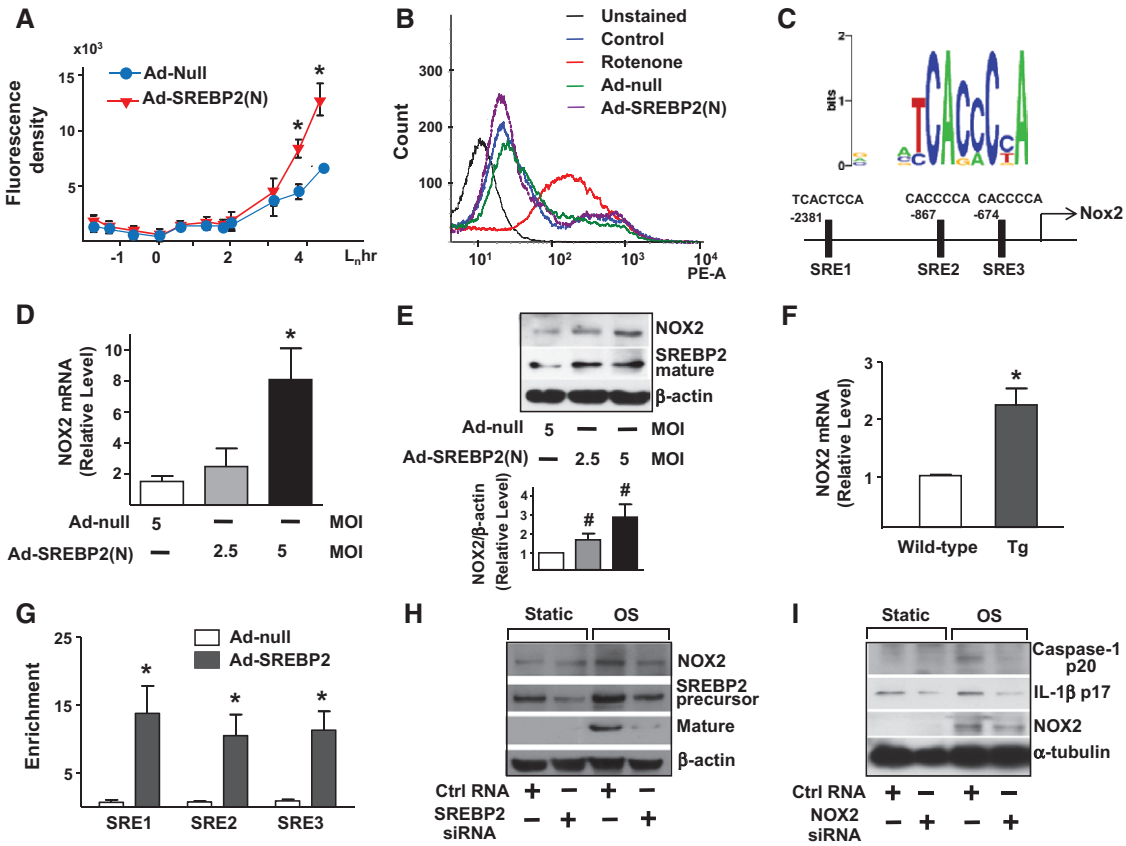

Figure 3. Sterol regulatory element binding protein 2 (SREBP2) upregulates NADPH oxidase 2 (NOX2) with an attendant increase in reactive oxygen species (ROS) in endothelial cells (ECs). **A**, ROS production monitored by measuring H2DCFDA fluorescence in human umbilical vein ECs (HUVECs) infected with adenovirus-null (Ad-null) or Ad-SREBP2(N) (5 multiplicities of infection [MOI]). **B**, Cytometric analysis of HUVECs infected with Ad-null or Ad-SREBP2(N) (5 MOI) for 48 hours or treated with rotenone (40 μmol/L) for 3 hours and then stained with MitoSOX for 30 minutes. **C**, Depiction of the 3 putative SRE binding sites, at −2381/−2367 (SRE1), −867/−861 (SRE2), and −674/668 (SRE3) bp upstream of the transcription initiation site in the human *NOX2* promoter. NOX2 mRNA levels (**D**) and representative immunoblot (and quantification) of NOX2 and the cleaved SREBP2 (**E**) in HUVECs treated with Ad-null (5 MOI) or Ad-SREBP2(N) (2.5 or 5 MOI). **F**, NOX2 mRNA levels in lung ECs from wild-type or EC-SREBP2(N)-Tg mice (n=8). **G**, Chromatin immunoprecipitation analysis with antibodies against SREBP2 or IgG, soluble chromatin (≈500 bp in length) from HUVECs infected with Ad-null or Ad-SREBP2(N), and primers targeting the region spanning the 3 SRE binding sites in the *NOX2* promoter. **H**, Representative immunoblot of NOX2, SREBP2 precursor, and mature form of SREBP2 in HUVECs transfected with 20 nmol/L control RNA or SREBP2 siRNA for 48 hours and then exposed to static or oscillatory shear flow (OS) for 14 hours. **I**, Representative immunoblot of caspase-1 p20, interleukin (IL)-1β p17, and NOX2 in HUVECs transfected with 20 nmol/L control RNA or NOX2 siRNA for 48 hours and then exposed to static or OS for 14 hours. At least 3 independent experiments were performed; results are mean±SEM. The Mann-Whitney *U* test with the exact method was used. **P*<0.05 vs Ad-null or wild-type; #*P*=0.05.

Therefore, the OS-activated SREBP2 transactivates NLRP3 in ECs.

SREBP2(N) Overexpression Enhances Endothelial Inflammation

IL-1β stimulates the expression of chemokines, for example, monocyte chemoattractant protein 1, and adhesion molecules, for example, vascular cell adhesion molecule 1 and E-selectin, in ECs, which enhances leukocyte-endothelium interactions. In agreement with increased IL-1β secretion via SREBP2-augmented inflammasome, SREBP2(N) overexpression increased the mRNA levels of monocyte chemoattractant protein 1, vascular cell adhesion molecule 1, and E-selectin (Figure 5A). Increased expression of monocyte chemoattractant protein 1 and adhesion molecules was also found in ECs isolated from EC-SREBP2(N)-Tg mice compared with wild-type littermates (Figure 5B). The SREBP2(N)-induced inflammation in ECs was associated with increased monocyte association, which was attenuated with caspase-1 inhibitor or NOX2 or NLPR3 siRNA knockdown (Figure 5C and 5D). Thus, NLRP3 inflammasome induced by OS via SREBP2 is functionally linked to endothelial proinflammatory responses.

SREBP2-NOX2-Inflammasome Activation in Atheroprone Regions of the Mouse Aorta

We next investigated whether the differential regulation of SREBP2 by PS and OS in ECs cultured in the flow channel also translated to a functional or functionally disturbed endothelium in atheroprotective versus atheroprone regions in the mouse arterial tree. As shown in Figure 6A and 6B, the activation of NLRP3 inflammasome was evident in the aortic arch, where the endothelium is exposed predominantly to disturbed flow.[23] As expected, the levels of the cleaved caspase-1 and IL-1β, that is, IL-1β p17, were higher in the aortic arch than in the thoracic aorta (Figure 6B). Consistent with this observation, the expression of IL-1β–regulated genes, that is,

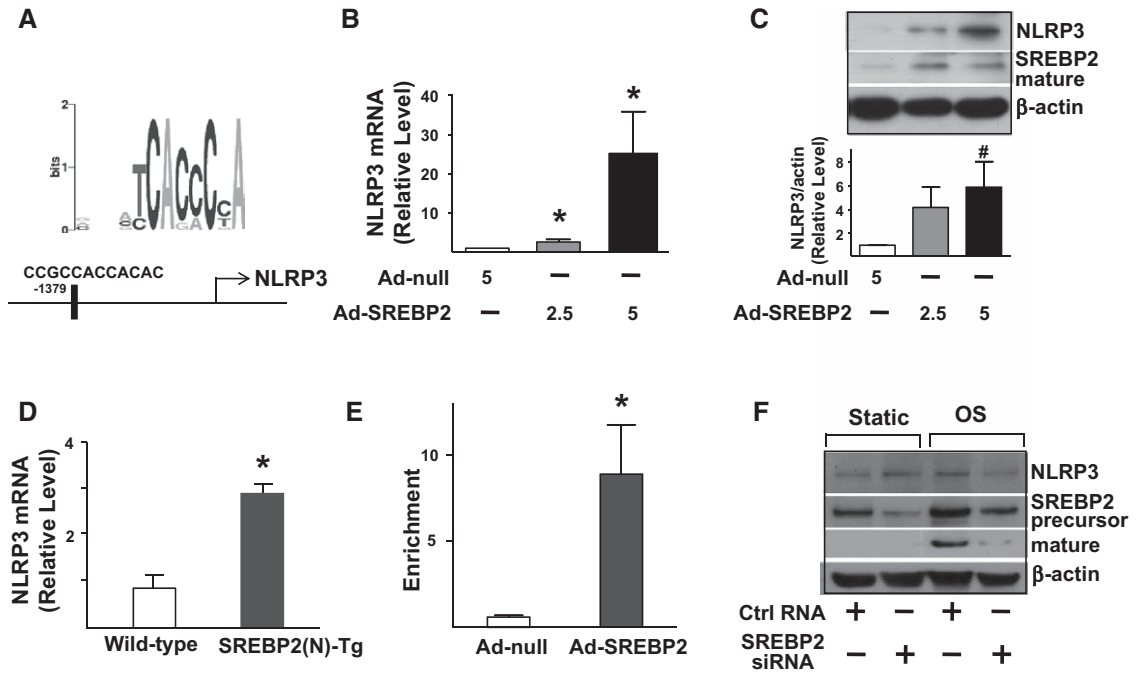

Figure 4. Sterol regulatory element binding protein 2 (SREBP2) overexpression upregulates NLRP3 inflammasome. **A**, Depiction of the putative SRE binding site located at −1379/−1368 bp upstream of the transcription initiation site in the human NLRP3 promoter. NLRP3 mRNA levels (**B**) and representative immunoblot (and quantification) of NLRP3 and the mature form of SREBP2 (**C**) in human umbilical vein endothelial cells (HUVECs) treated with adenovirus-null (Ad-null; 5 multiplicities of infection [MOI]) or Ad-SREBP2(N) (2.5 or 5 MOI). **D**, NLRP3 mRNA levels in lung ECs from wild-type or EC-SREBP2(N)-Tg mice (n=8). **E**, Chromatin immunoprecipitation analysis with antibodies against SREBP2 or IgG, soluble chromatin from HUVECs infected with Ad-null or Ad-SREBP2(N), and primers targeting the region spanning the SRE binding site in the *NLRP3* promoter. **F**, Representative immunoblot of NLRP3, precursor SREBP2, and mature form of SREBP2 in HUVECs transfected with 20 nmol/L control RNA or SREBP2 siRNA for 48 hours and then exposed to static conditions or oscillatory shear flow (OS) for 14 hours. Bar graphs represent mean±SEM from at least 3 independent experiments. The Mann-Whitney *U* test with the exact method was used. **P*<0.05 vs Ad-null or wild-type; #*P*=0.05 vs Ad-null.

monocyte chemoattractant protein 1, vascular cell adhesion molecule 1, intercellular adhesion molecule 1, and E-selectin, was increased in the aortic arch (Figure 6A). In addition, we separated intima (endothelium) from media and adventitia of thoracic aorta and aortic arch of C57BL/6 mice. As illustrated in Figure 6C, the expression levels of SREBP2, NOX2, and NLRP3 in the isolated endothelium in aortic arch were higher than those in thoracic aorta. Importantly, no differences were found between thoracic aorta and aortic arch in tissues containing media and adventitia. Higher levels of NLRP3, NOX2, and SREBP2 in the aortic arch were also verified by in situ hybridization (Figure IV in the online-only Data Supplement). Thus, the NLPR3 inflammasome is activated in the endothelium of atheroprone region of the arterial tree in vivo.

EC-specific SREBP2(N) overexpression mimicking OS induction of SREBP2 should render the thoracic aorta of EC-SREBP2(N)-Tg mice atheroprone. As expected, activation of NLRP3 inflammasome and induction of chemoattractants and adhesion molecules were seen in these arterial segments compared with corresponding areas in wild-type littermates (Figure 6D). SREBP2(N) overexpression also caused a functionally disturbed endothelium, as evidenced by impaired vasodilation responding to flow (Figure V in the online-only Data Supplement).

SREBP2(N) Overexpression in ECs Predisposes Atherosclerosis

We introduced the ApoE-null background into EC-SREBP2(N)-Tg mice to investigate whether EC-specific overexpression of SREBP2(N) leads to atherogenesis in atheroprotective regions in ApoE$^{-/-}$/EC-SREBP2(N) mice. After 8 weeks of an atherogenic diet, the levels of total cholesterol and LDL were comparable between ApoE$^{-/-}$/EC-SREBP2(N) mice and their ApoE$^{-/-}$ littermates (Table 1). However, the mean lesion area in thoracic aortas was ≈1.5-fold larger for ApoE$^{-/-}$/EC-SREBP2(N)-Tg than ApoE$^{-/-}$ mice (17.4±1.7% versus 11.5±1.3%; Figure 7A and 7C). The mean lesion area in the aortic arch was also larger for ApoE$^{-/-}$/EC-SREBP2(N) than ApoE$^{-/-}$ mice (47.7±2.5% versus 39.7±3.1%). The order of lesion size was as follows: aortic arch of ApoE$^{-/-}$/EC-SREBP2(N) mice>aortic arch of ApoE$^{-/-}$ mice>thoracic aorta of ApoE$^{-/-}$/EC-SREBP2(N) mice>thoracic aorta of ApoE$^{-/-}$ mice. The total lesion area as a sum of aortic arch, thoracic aorta, plus abdominal aorta remained greater for ApoE$^{-/-}$/EC-SREBP2(N) mice than control littermates (22.5±1.4% versus 18.2±1.5%). These results demonstrate that local flow patterns synergize with other atherogenic factors, for example, hyperlipidemia, in the formation of atherosclerotic lesions. We also compared the lesion development in the 2 groups of animals fed normal chow for 24 weeks. As expected, the serum levels of total cholesterol and LDL were significantly lower with normal chow than with an atherogenic diet (Table 1). Compared with the ApoE$^{-/-}$ littermates, ApoE$^{-/-}$/EC-SREBP2(N) mice showed more lesions in aortic arches, particularly the inner curvature of the arch and the orifices of the arch vessels (Figure 7B and 7D). Previous studies by others showed that these areas have elevated nuclear

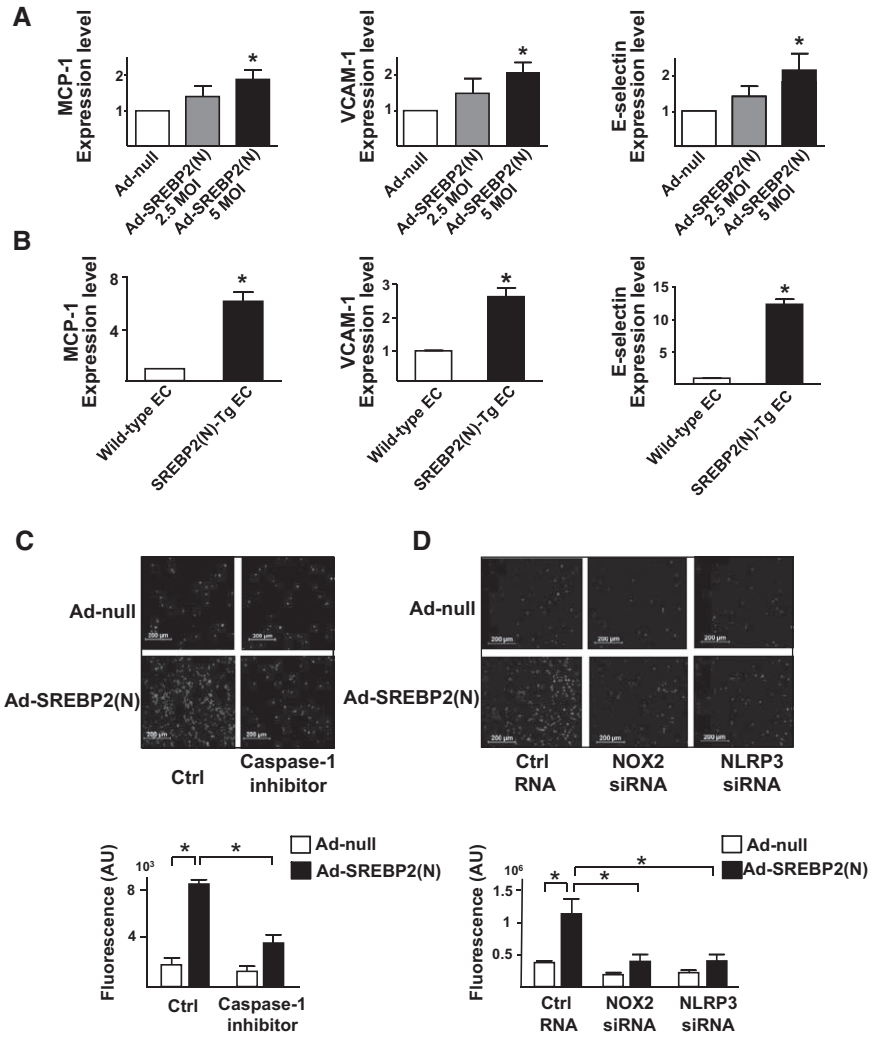

Figure 5. Increased level of sterol regulatory element binding protein 2 (SREBP2) causes endothelial cell (EC) NLRP3 inflammation. **A**, Quantification of mRNA levels of monocyte chemoattractant protein 1 (MCP-1), vascular cell adhesion molecule 1 (VCAM-1), and E-selectin in human umbilical vein endothelial cells (HUVECs) treated with adenovirus-null (Ad-null; 5 multiplicities of infection [MOI]) or Ad-SREBP2(N) (2.5 or 5 MOI) or (**B**) in lung ECs from wild-type or EC-SREBP2(N)-Tg mice (n=8). **C** and **D**, HUVECs were infected with Ad-null or Ad-HA-SREBP2(N) for 24 hours and then treated with or without caspase-1 inhibitor Z-YVAD-FMK (2 μmol/L) for 24 hours. In separate experiments, HUVECs were transfected with control RNA, NADPH oxidase 2 (NOX2) siRNA, or NLRP3 siRNA and then infected with Ad-null or Ad-HA-SREBP2(N) for 24 hours. The cells were incubated for 30 minutes with LeukoTracker-labeled THP1 cells. For quantification, parallel batches of treated cells were lysed and the fluorescence was measured. Data are mean±SEM from 3 independent experiments performed in triplicate. The Mann-Whitney *U* test with the exact method was used. **P*<0.05 for comparisons with Ad-null or wild-type ECs.

factor-κB and vascular cell adhesion molecule 1 activation.[23,24] Of note, with normal chow, lesion areas were marginal in the thoracic aortas of both ApoE$^{-/-}$/EC-SREBP2(N) and ApoE$^{-/-}$ mice, which reiterates the notion that hyperlipidemia synergizes with hemodynamic forces in the origin of atherosclerosis.

Discussion

The "response-to-injury" hypothesis states that endothelial dysfunction precedes the development of atherosclerosis.[25] Much evidence suggests that atheroprone flow patterns in the conduit arteries are a determining factor of atherogenesis. Furthermore, the Pathological Determinants of Atherosclerosis in Youth (PDAY) study provides unequivocal evidence that cardiovascular risk factors (eg, hyperlipidemia, smoking, and hypertension) exacerbate atherosclerosis in atheroprone areas in the human arterial tree.[26,27] Here, we report that disturbed flow applied to ECs induced NLRP3 inflammasome via SREBP2 activation. Such SREBP2 activation of NLRP3 inflammasome is sufficient for functionally disturbed endothelium leading to atherogenesis as supported by mouse models harboring the EC-SREBP2(N) transgene. Differential development of atherosclerotic lesions in the aortic arch compared with thoracic aorta in mice with or without EC-specific expression of SREBP2(N) and in the presence or absence of an atherogenic diet (Figure 7) provides a molecular basis for the hemodynamic-induced atherosclerosis susceptibility seen in the human arterial tree. We reasoned that endothelial expression of SREBP2(N) mimicking the effect of disturbed flow synergizes with hyperlipidemia (caused by an ApoE$^{-/-}$ background together with an atherogenic diet) to accelerate atherosclerosis. The thesis is further supported by experiments using EC-SREBP2(N)-Tg or wild-type C57BL6 mice fed an atherogenic diet. Early atherosclerotic plaques developed in the aortic root of EC-SREBP2(N)-Tg mice but not control littermate mice (Figure VI in the online-only Data Supplement and Table 2). Thus, the translational relevance of this study is that the spatial localization and severity of atherosclerosis can depend on atheroprone flow coupled with cardiovascular risk factors via SREBP2(N)-induced NLRP3 inflammasome.

Clearly, IL-1β is a major atheroprone factor.[28] Atherosclerosis was decreased in several rodent models lacking IL-1β or type I IL-1 receptor.[29,30] In contrast, mice deficient in IL-1 receptor antagonist show increased atherosclerosis.[31] Canakinumab, an anti-human IL-1β monoclonal antibody, is currently being used in the Canakinumab

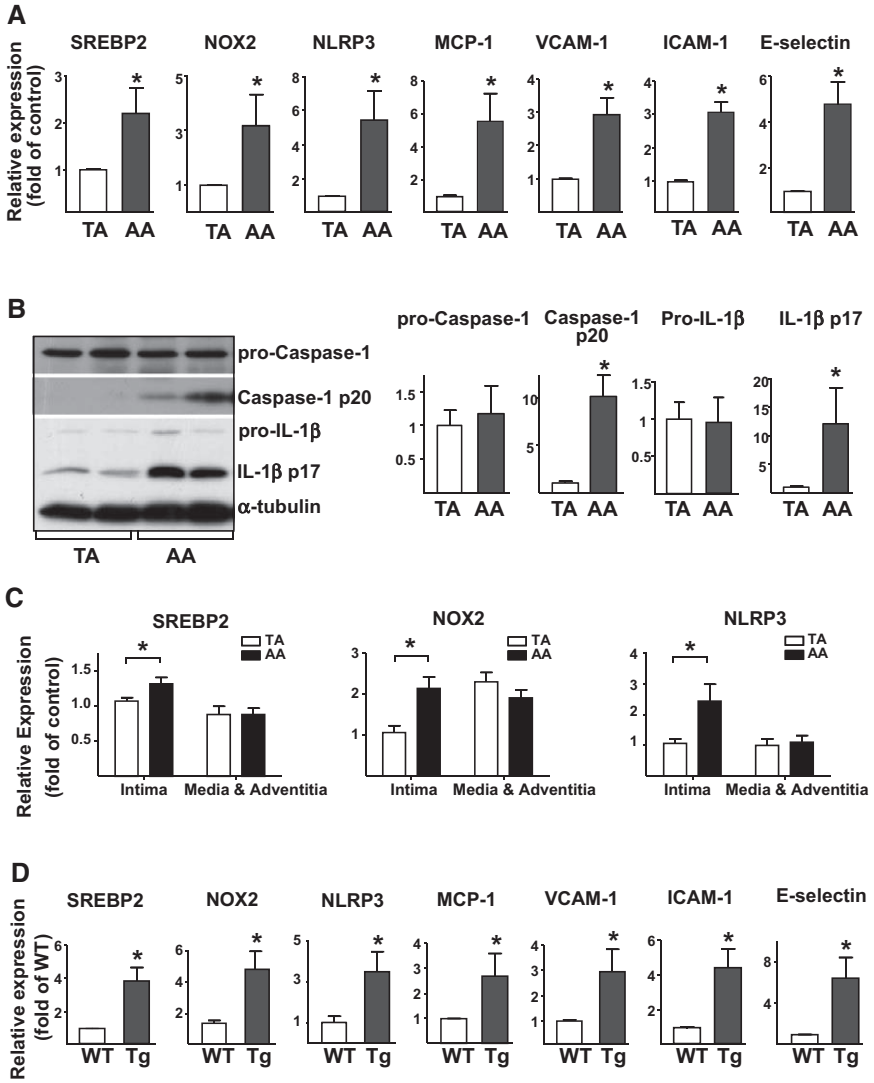

Figure 6. Sterol regulatory element binding protein 2 (SREBP2)–NADPH oxidase 2 (NOX2)–inflammasome activation in atheroprone regions of mouse aortas. **A**, Quantification of mRNA levels of SREBP2, NOX2, NLRP3, monocyte chemoattractant protein 1 (MCP-1), vascular cell adhesion molecule 1 (VCAM-1), intercellular adhesion molecule 1 (ICAM-1), and E-selectin in the thoracic aorta (TA) and aortic arch (AA) of C57BL/6 mice (n=7). **B**, Representative immunoblot of procaspase-1, caspase-1 p20, pro–interleukin (IL)-1β, and IL-1β p17 in TA and AA from C57BL/6 mice. **C**, The levels of SREBP2, NOX2, and NLRP3 mRNA in aortic intima or media and adventitia. Data are mean±SEM of the relative mRNA normalized to that of β-actin (n=18). **D**, Quantification of mRNA levels of SREBP2, NOX2, NLRP3, MCP-1, VCAM-1, ICAM-1, and E-selectin in TA from wild-type (n=7) and EC-SREBP2(N)-Tg mice (n=7). The Mann-Whitney *U* test with the exact method was used. **P*<0.05 for comparisons with TA or WT.

Anti-inflammatory Thrombosis Outcomes Study (CANTOS) to assess the efficacy of anti-IL-1β in reducing cardiovascular events.[32] The antiatherosclerosis effect resulting from IL-1β antagonism should involve the inhibition of NLRP3 inflammasome in the endothelium and should be experimentally verified. Undoubtedly, NLRP3 inflammasome in monocyte/macrophage is important for atherosclerosis, as suggested by transplantation experiments with bone marrow deficient in NLRP3, ASC, or IL-1α/β.[9] However, this macrophage-associated mechanism would not contribute to functionally disturbed endothelium and ensuing atherosclerosis in our mouse models because the SREBP2(N) transgene was expressed only in ECs, not in bone marrow–derived macrophages (Figure VII in the online-only Data Supplement).

Table 1. Serum Lipid Profile of ApoE$^{-/-}$/EC-SREBP2(N) and Their ApoE$^{-/-}$ Littermates Fed a Normal Chow or an Atherogenic Diet

	Normal Chow, mg/dL*		Atherogenic Diet, mg/dL†	
Serum Lipids	ApoE$^{-/-}$ (n=7)	ApoE$^{-/-}$/EC-SREBP2(N) (n=6)	ApoE$^{-/-}$ (n=17)	ApoE$^{-/-}$/EC-SREBP2(N) (n=18)
Total cholesterol	1284±272‡	1224±334	1806±298	1967±576
Triglycerides	169±49	197±112	111±57	125±89
LDL	490±54	478±83	1055±168	1035±235
VLDL	30±14	39±22	21±12	29±22
HDL	764±253	707±374	730±177	903±365

EC indicates endothelial cell; HDL, high-density lipoprotein; LDL, low-density lipoprotein; SREBP2, sterol regulatory element binding protein 2; and VLDL, very-low-density lipoprotein.

*Normal chow group was 24-week-old mice fed a normal chow.

†Atherogenic diet group was 8-week-old mice fed an atherogenic diet for 8 weeks.

‡All values are expressed as mean±SD averaged from the number of animals as indicated.

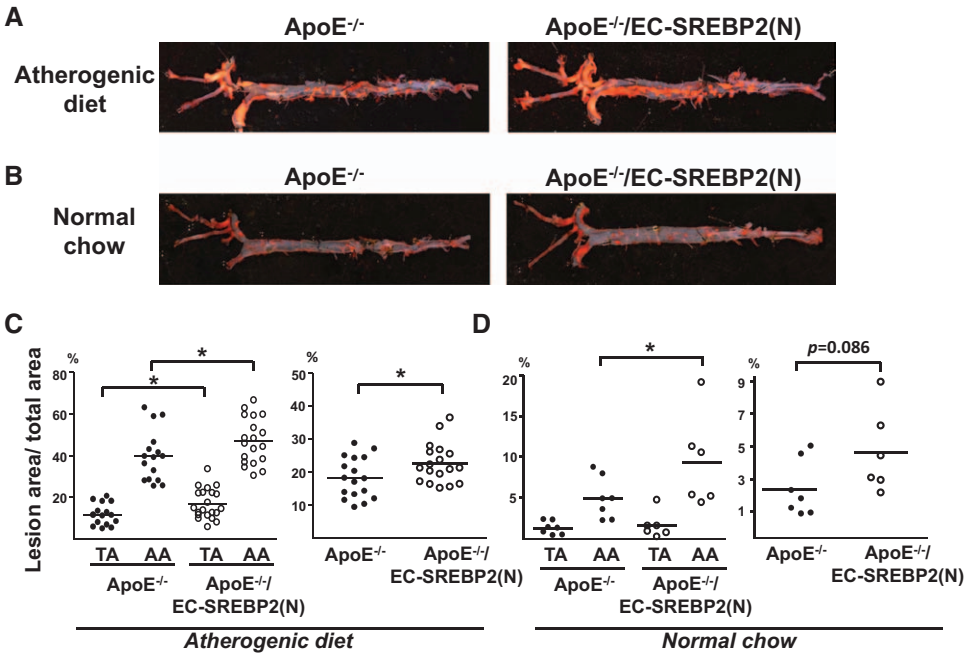

Figure 7. Overexpression of sterol regulatory element binding protein 2 (SREBP2) in endothelial cells (ECs) enhances atherosclerosis. **A**, Representative Oil Red O staining of aortas from (**A**) 8-week-old ApoE$^{-/-}$ (n=17) and ApoE$^{-/-}$/SREBP2(N) mice (n=18) fed a high-fat diet for 8 weeks and (**B**) 24-week-old ApoE$^{-/-}$ (n=7) and ApoE$^{-/-}$/SREBP2(N) mice (n=6) fed a normal chow. **C** and **D**, Quantification of percent lesion areas in the thoracic aorta (TA), aortic arch (AA), and whole aorta from groups in **A** and **B**. The Student *t* test or Mann-Whitney *U* test with the exact method was used. *P<0.05.

Reconciling published literature with the present report, we propose that the disturbed flow–increased NLRP3 inflammasome in ECs and consequent production and secretion of IL-1β create a focal gradient of inflammatory cytokines and chemoattractants. This flow-elicited proinflammatory milieu recruits sentinel cells (ie, monocytes) and facilitates the retention and differentiation of monocytes in the subendothelial space. Indeed, atherosclerosis was found to be substantially lower in ApoE$^{-/-}$/IL-1β$^{-/-}$ than ApoE$^{-/-}$/IL-1β$^{+/+}$ thoracic aortas.[30]

In macrophages, the SREBP2-coinduced miR-33a targets ABCA1, which impairs reverse cholesterol transport.[5,6] An antigomir against miR-33 decreases atherosclerosis in LDL receptor–null mice, with a concomitant increase in the level of high-density lipoprotein.[33] Inhibition of miR-33 also increases the level of high-density lipoprotein and lowers that of very LDL triglycerides in nonhuman primates.[34] In line with SREBP2 induction, OS-induced miR-33a targets ABCA1 in ECs (Figure 1). Given that cholesterol crystals are an inflammasome inducer,[9] disturbed flow patterns should increase the cholesterol level, which arguably synergizes with SREBP2 to activate NLPR3 inflammasome. Conversely, the atheroprotective flow patterns should induce liver X receptors and hence upregulate ABCA1 to facilitate reverse cholesterol transport.[35] Civelek et al[36] reported no site-specific differences in endothelial ABCA1 expression between susceptible and protected sites of swine arteries. However, our published work showed that ABCA1 level is lower in the mouse aortic arch compared with thoracic aorta.[35] The possible reason for the discrepancy is the different species and diets used in the 2 studies. Given that hypercholesterolemia significantly increased ABCA1 expression in swine endothelium, it might be difficult to detect a site-specific difference in endothelial ABCA1 expression.

Table 2. Serum Lipid Profile of EC-SREBP2(N) and Their Wild-Type Littermates Fed an Atherogenic Diet

Serum Lipids	Wild-Type, mg/dL (n=5)	EC-SREBP2(N), mg/dL (n=5)
Total cholesterol	161±6*	176±30
Triglyceride	56±13	59±11
LDL	16±4	12±2
VLDL	105±31	107±20
HDL	62±36	68±20

EC indicates endothelial cell; HDL, high-density lipoprotein; LDL, low-density lipoprotein; SREBP2, sterol regulatory element binding protein 2; and VLDL, very-low-density lipoprotein.

*All values are expressed as mean±SD averaged from the number of animals as indicated.

The intracellular and extracellular levels of sterols intricately regulate SREBP2, which in turn modulates cellular cholesterol homeostasis.[4] Significantly, excessive amounts of 25-HC do not prevent OS induction of SREBP2 (Figure 1G), suggesting that the mechanotransduction mechanism overrides that of the cholesterol-sensing system, leading to sustained SREBP2 activation. Thus, the disturbed flow–activated SREBP2 appears to disrupt cholesterol homeostasis in its activation of inflammasome. This argument can explain the synergism between atheroprone flow and hyperlipidemia in inducing atherosclerosis.

The endoplasmic reticulum stress/unfolded protein response is activated in ECs by atheroprone flow in vitro[37] and is upregulated in endothelium of swine atheroprone sites in vivo.[38] We have

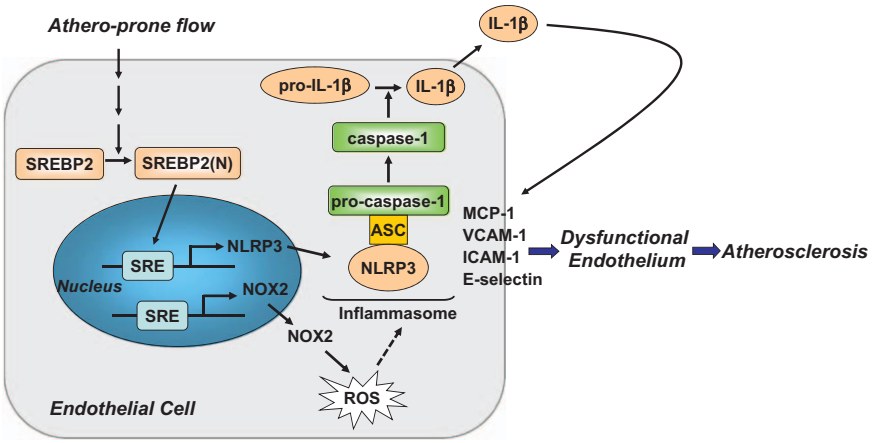

Figure 8. Graphic summary of the mechanism for sterol regulatory element binding protein 2 (SREBP2) activation of NLRP3 inflammasome in endothelium mediates atheroprone flow-induced atherosclerosis. ICAM-1, intercellular adhesion molecule 1; IL, interleukin; MCP-1, monocyte chemoattractant protein 1; NOX2, NADPH oxidase 2; ROS, reactive oxygen species; and VCAM-1. vascular cell adhesion molecule 1.

previously shown that the unfolded protein response chaperone ATF6 inhibits SREBP2 activity by binding to SREBP2 in liver cells under glucose deprivation.[14] This inhibitory effect does not involve ATF6 regulation of SREBP2 maturation, that is, cleavage. In contrast, OS affects SREBP2 cleavage (Figure 1A). Support for the 2 distinct mechanisms of SREBP2 regulation comes from experiments showing that ATF6 and SREBP2 were coinduced in ECs under OS and that ATF6 knockdown by siRNA did not affect SREBP2 induction by OS (data not shown).

Among mechanosensitive signaling molecules, Akt and adenosine monophosphate–activated protein kinase regulate the endothelial phenotypic changes responding to atheroprone and atheroprotective flow, respectively.[39] Akt positively regulates SREBP[40] through direct phosphorylation and transcriptional activation via mTORC1. On the other hand, adenosine monophosphate–activated protein kinase inhibits SREBP-1c and -2 activities through Ser372 phosphorylation, which inhibits SREBP cleavage, nuclear translocation, and transcriptional activity.[41] Thus, the disturbed flow–activated Akt is likely involved in SREBP2 activation in atheroprone areas, whereas SREBP2 suppression in atheroresistant areas is mediated at least in part by adenosine monophosphate–activated protein kinase. Thus, adenosine monophosphate–activated protein kinase activators such as statin and metformin may play a beneficial role similar to that of atheroprotective flow in phosphorylating SREBP2.

SREBP-1a is involved in the lipopolysaccharide-stimulated IL-1β production through activation of NLRP1a inflammasome in macrophages.[19] The *SREBP1* promoter region also contains an SRE binding site, which can be regulated by SREBP2.[42] The OS-induced SREBP2 should also activate SREBP1 because ECs transfected with Ad-SREBP2(N) showed an increased expression of SREBP1 (Figure VIII in the online-only Data Supplement). However, we did not find increased levels of NLRP1a in ECs from EC-SREBP2(N)-Tg mice (Figure VIII in the online-only Data Supplement). Most, if not all, NLRP3 activators upregulate NOXs, with concurrent elevation of the short-lived ROS, so NOX-mediated redox signaling is involved in NLRP3 inflammasome activation.[20,21] Nevertheless, NOXs are not necessary for inflammasome activation in hematopoietic cells because immune cells deficient in NOXs show normal or hyperactive activation of inflammasome.[43,44] In contrast, our data in Figure 3 suggest that SREBP2 transactivation of NOX2 is necessary for inducing NLRP3 inflammasome in ECs. Although the molecular basis of the discrepancies between macrophages and ECs remains unknown, SREBP2 induction of NOX2 is implicated in endothelial biology in that the major enzymatic product of NOX2 is ROS.[45]

As summarized in Figure 8, we demonstrated that atheroprone flow, like endogenous damage- and pathogen-associated molecules such as cholesterol crystals and lipopolysaccharide, induces NLRP3 inflammasome in endothelium via SREBP2 activation. This increased innate immunity in endothelium synergizes with hyperlipidemia to result in the focal nature of atherosclerosis.

Sources of Funding

This work was supported in part by National Institutes of Health grants HL89940 and HL105318, National Natural Science Foundation of China grant 81270349, National Science Council of the Republic of China (NSC 101-2311-B-009-003-MY3 and NSC 100-2627-B-009-002) and UST-UCSD I-RiCE Program (NSC 101-2911-I-009-101).

Disclosures

None.

References

1. Ross R. Mechanisms of disease: atherosclerosis: an inflammatory disease. *N Engl J Med*. 1999;340:115–126.
2. Chiu JJ, Chien S. Effects of disturbed flow on vascular endothelium: pathophysiological basis and clinical perspectives. *Physiol Rev*. 2011;91:327–387.
3. Davies PF. Hemodynamic shear stress and the endothelium in cardiovascular pathophysiology. *Nat Clin Pract Cardiovasc Med*. 2009;6:16–26.
4. Espenshade PJ, Hughes AL. Regulation of sterol synthesis in eukaryotes. *Annu Rev Genet*. 2007;41:401–427.
5. Najafi-Shoushtari SH, Kristo F, Li Y, Shioda T, Cohen DE, Gerszten RE, Näär AM. MicroRNA-33 and the SREBP host genes cooperate to control cholesterol homeostasis. *Science*. 2010;328:1566–1569.
6. Rayner KJ, Suárez Y, Dávalos A, Parathath S, Fitzgerald ML, Tamehiro N, Fisher EA, Moore KJ, Fernández-Hernando C. MiR-33 contributes to the regulation of cholesterol homeostasis. *Science*. 2010;328:1570–1573.
7. Liu Y, Chen BP, Lu M, Zhu Y, Stemerman MB, Chien S, Shyy JY. Shear stress activation of SREBP1 in endothelial cells is mediated by integrins. *Arterioscler Thromb Vasc Biol*. 2002;22:76–81.
8. Wen H, Ting JP, O'Neill LA. A role for the NLRP3 inflammasome in metabolic diseases: did Warburg miss inflammation? *Nat Immunol*. 2012;13:352–357.
9. Duewell P, Kono H, Rayner KJ, Sirois CM, Vladimer G, Bauernfeind FG, Abela GS, Franchi L, Nuñez G, Schnurr M, Espevik T, Lien E, Fitzgerald KA, Rock KL, Moore KJ, Wright SD, Hornung V, Latz E. NLRP3 inflammasomes are required for atherogenesis and activated by cholesterol crystals. *Nature*. 2010;464:1357–1361.
10. Rajamäki K, Lappalainen J, Oörni K, Välimäki E, Matikainen S, Kovanen PT, Eklund KK. Cholesterol crystals activate the NLRP3 inflammasome

in human macrophages: a novel link between cholesterol metabolism and inflammation. *PLoS One*. 2010;5:e11765.
11. Hwang J, Ing MH, Salazar A, Lassègue B, Griendling K, Navab M, Sevanian A, Hsiai TK. Pulsatile versus oscillatory shear stress regulates NADPH oxidase subunit expression: implication for native LDL oxidation. *Circ Res*. 2003;93:1225–1232.
12. Lim YC, Luscinskas FW. Isolation and culture of murine heart and lung endothelial cells for in vitro model systems. *Methods Mol Biol*. 2006;341:141–154.
13. Zhang Y, Lee TS, Kolb EM, Sun K, Lu X, Sladek FM, Kassab GS, Garland T Jr, Shyy JY. AMP-activated protein kinase is involved in endothelial NO synthase activation in response to shear stress. *Arterioscler Thromb Vasc Biol*. 2006;26:1281–1287.
14. Zeng L, Lu M, Mori K, Luo S, Lee AS, Zhu Y, Shyy JY. ATF6 modulates SREBP2-mediated lipogenesis. *EMBO J*. 2004;23:950–958.
15. Wingender E, Karas H, Knuppel R. TRANSFAC database as a bridge between sequence data libraries and biological function. *Pac Symp Biocomput*. 1997;2:477–485.
16. Ni ZF, Ng DW, Liu JX, Chen ZJ. Chromatin immunoprecipitation (ChIP) assay. *Protocol Exchange*. 2009. doi:10.1038/nprot.2009.11. http://www.nature.com/protocolexchange/protocols/500. Accessed July 2, 2013.
17. Nakano K, Egashira K, Ohtani K, Gang Z, Iwata E, Miyagawa M, Sunagawa K. Azelnidipine has anti-atherosclerotic effects independent of its blood pressure-lowering actions in monkeys and mice. *Atherosclerosis*. 2008;196:172–179.
18. Nigro P, Abe J, Berk BC. Flow shear stress and atherosclerosis: a matter of site specificity. *Antioxid Redox Signal*. 2011;15:1405–1414.
19. Im SS, Yousef L, Blaschitz C, Liu JZ, Edwards RA, Young SG, Raffatellu M, Osborne TF. Linking lipid metabolism to the innate immune response in macrophages through sterol regulatory element binding protein-1a. *Cell Metab*. 2011;13:540–549.
20. Dostert C, Pétrilli V, Van Bruggen R, Steele C, Mossman BT, Tschopp J. Innate immune activation through Nalp3 inflammasome sensing of asbestos and silica. *Science*. 2008;320:674–677.
21. Zhou R, Tardivel A, Thorens B, Choi I, Tschopp J. Thioredoxin-interacting protein links oxidative stress to inflammasome activation. *Nat Immunol*. 2010;11:136–140.
22. Matlung HL, Bakker EN, VanBavel E. Shear stress, reactive oxygen species, and arterial structure and function. *Antioxid Redox Signal*. 2009;11:1699–1709.
23. Suo J, Ferrara DE, Sorescu D, Guldberg RE, Taylor WR, Giddens DP. Hemodynamic shear stresses in mouse aortas: implications for atherogenesis. *Arterioscler Thromb Vasc Biol*. 2007;27:346–351.
24. Hajra L, Evans AI, Chen M, Hyduk SJ, Collins T, Cybulsky MI. The NF-kappa B signal transduction pathway in aortic endothelial cells is primed for activation in regions predisposed to atherosclerotic lesion formation. *Proc Natl Acad Sci U S A*. 2000;97:9052–9057.
25. Landmesser U, Hornig B, Drexler H. Endothelial function: a critical determinant in atherosclerosis? *Circulation*. 2004;109(suppl 1):II27–II33.
26. McGill HC Jr, McMahan CA, Herderick EE, Tracy RE, Malcom GT, Zieske AW, Strong JP. Effects of coronary heart disease risk factors on atherosclerosis of selected regions of the aorta and right coronary artery: PDAY Research Group: Pathobiological Determinants of Atherosclerosis in Youth. *Arterioscler Thromb Vasc Biol*. 2000;20:836–845.
27. McGill HC Jr, McMahan CA, Gidding SS. Preventing heart disease in the 21st century: implications of the Pathobiological Determinants of Atherosclerosis in Youth (PDAY) study. *Circulation*. 2008;117:1216–1227.
28. Fearon WF, Fearon DT. Inflammation and cardiovascular disease: role of the interleukin-1 receptor antagonist. *Circulation*. 2008;117:2577–2579.
29. Chamberlain J, Evans D, King A, Dewberry R, Dower S, Crossman D, Francis S. Interleukin-1beta and signaling of interleukin-1 in vascular wall and circulating cells modulates the extent of neointima formation in mice. *Am J Pathol*. 2006;168:1396–1403.
30. Kirii H, Niwa T, Yamada Y, Wada H, Saito K, Iwakura Y, Asano M, Moriwaki H, Seishima M. Lack of interleukin-1beta decreases the severity of atherosclerosis in ApoE-deficient mice. *Arterioscler Thromb Vasc Biol*. 2003;23:656–660.
31. Devlin CM, Kuriakose G, Hirsch E, Tabas I. Genetic alterations of IL-1 receptor antagonist in mice affect plasma cholesterol level and foam cell lesion size. *Proc Natl Acad Sci U S A*. 2002;99:6280–6285.
32. Ridker PM, Thuren T, Zalewski A, Libby P. Interleukin-1β inhibition and the prevention of recurrent cardiovascular events: rationale and design of the Canakinumab Anti-inflammatory Thrombosis Outcomes Study (CANTOS). *Am Heart J*. 2011;162:597–605.
33. Rayner KJ, Sheedy FJ, Esau CC, Hussain FN, Temel RE, Parathath S, van Gils JM, Rayner AJ, Chang AN, Suarez Y, Fernandez-Hernando C, Fisher EA, Moore KJ. Antagonism of miR-33 in mice promotes reverse cholesterol transport and regression of atherosclerosis. *J Clin Invest*. 2011;121:2921–2931.
34. Rayner KJ, Esau CC, Hussain FN, McDaniel AL, Marshall SM, van Gils JM, Ray TD, Sheedy FJ, Goedeke L, Liu X, Khatsenko OG, Kaimal V, Lees CJ, Fernandez-Hernando C, Fisher EA, Temel RE, Moore KJ. Inhibition of miR-33a/b in non-human primates raises plasma HDL and lowers VLDL triglycerides. *Nature*. 2011;478:404–407.
35. Zhu M, Fu Y, Hou Y, Wang N, Guan Y, Tang C, Shyy JY, Zhu Y. Laminar shear stress regulates liver X receptor in vascular endothelial cells. *Arterioscler Thromb Vasc Biol*. 2008;28:527–533.
36. Civelek M, Grant GR, Irolla CR, Shi C, Riley RJ, Chiesa OA, Stoeckert CJ Jr, Karanian JW, Pritchard WF, Davies PF. Prelesional arterial endothelial phenotypes in hypercholesterolemia: universal ABCA1 upregulation contrasts with region-specific gene expression in vivo. *Am J Physiol Heart Circ Physiol*. 2010;298:H163–H170.
37. Feaver RE, Hastings NE, Pryor A, Blackman BR. GRP78 upregulation by atheroprone shear stress via p38-, alpha2beta1-dependent mechanism in endothelial cells. *Arterioscler Thromb Vasc Biol*. 2008;28:1534–1541.
38. Civelek M, Manduchi E, Riley RJ, Stoeckert CJ Jr, Davies PF. Chronic endoplasmic reticulum stress activates unfolded protein response in arterial endothelium in regions of susceptibility to atherosclerosis. *Circ Res*. 2009;105:453–461.
39. Guo D, Chien S, Shyy JY. Regulation of endothelial cell cycle by laminar versus oscillatory flow: distinct modes of interactions of AMP-activated protein kinase and Akt pathways. *Circ Res*. 2007;100:564–571.
40. Krycer JR, Sharpe LJ, Luu W, Brown AJ. The Akt-SREBP nexus: cell signaling meets lipid metabolism. *Trends Endocrinol Metab*. 2010;21:268–276.
41. Li Y, Xu S, Mihaylova MM, Zheng B, Hou X, Jiang B, Park O, Luo Z, Lefai E, Shyy JY, Gao B, Wierzbicki M, Verbeuren TJ, Shaw RJ, Cohen RA, Zang M. AMPK phosphorylates and inhibits SREBP activity to attenuate hepatic steatosis and atherosclerosis in diet-induced insulin-resistant mice. *Cell Metab*. 2011;13:376–388.
42. Amemiya-Kudo M, Shimano H, Yoshikawa T, Yahagi N, Hasty AH, Okazaki H, Tamura Y, Shionoiri F, Iizuka Y, Ohashi K, Osuga J, Harada K, Gotoda T, Sato R, Kimura S, Ishibashi S, Yamada N. Promoter analysis of the mouse sterol regulatory element-binding protein-1c gene. *J Biol Chem*. 2000;275:31078–31085.
43. Meissner F, Seger RA, Moshous D, Fischer A, Reichenbach J, Zychlinsky A. Inflammasome activation in NADPH oxidase defective mononuclear phagocytes from patients with chronic granulomatous disease. *Blood*. 2010;116:1570–1573.
44. van de Veerdonk FL, Smeekens SP, Joosten LA, Kullberg BJ, Dinarello CA, van der Meer JW, Netea MG. Reactive oxygen species-independent activation of the IL-1beta inflammasome in cells from patients with chronic granulomatous disease. *Proc Natl Acad Sci U S A*. 2010;107:3030–3033.
45. Takac I, Schröder K, Brandes RP. The Nox family of NADPH oxidases: friend or foe of the vascular system? *Curr Hypertens Rep*. 2012;14:70–78.

CLINICAL PERSPECTIVE

Atherosclerosis preferentially develops at branches and curvatures in the arterial tree, and the disturbed flow pattern imposed in the endothelium in these regions plays a major role in the preferentially localized atherosclerosis. In this study, we show that disturbed flow increases endothelial innate immunity via NLRP3 inflammasome in vitro and in vivo. The underlying mechanism involves the induction of sterol regulatory element binding protein 2 (SREBP2), which transactivates NADPH oxidase 2 and NLRP3. The increased innate immunity in endothelium predisposes hyperlipidemia to result in the focal nature of atherosclerosis. This newly defined SREBP2/NLRP3 inflammasome pathway suggests that SREBP2 could be a therapeutic target to prevent atherosclerosis initiation, which is in line with the antiatherosclerosis effect of interleukin-1β antagonism.

SUPPLEMENTAL MATERIALS

Supplemental methods

Isolation of Primary Mouse Lung Endothelial Cells

Isolation of primary mouse lung endothelial cells were performed as described previously [1]. Monoclonal rat anti-mouse CD31 antibody from BD Transduction Laboratory was covalently coupled to pre-washed Dynabeads® sheep anti-rat IgG during an overnight incubation. Lung tissue was excised, aseptically minced into 1 mm x 2 mm squares, digested with collagenase A at 37 ºC with gentle agitation for 45 min, triturated 12 times with a 30-cc syringe, and passed through a 70-μm disposable cell strainer (BD Falcon) into a 50 mL conical centrifuge tube. The cell suspension was then centrifuged at 400 × *g* for 8 min at 4 °C, and the pellet was resuspended in 2 mL of medium. Anti-CD31 coated beads were added to the cell suspension, mixed, and incubated for 10 min at room temperature. The bead-bound cells were isolated with a magnet, resuspended in growth medium M199, and plated on collagen-coated T75 flasks. At the following day, the flasks were washed with media to remove loosely adherent cells.

Immunoblotting

Cells or tissue samples were lysed with a buffer containing 10 mM Tris, pH 7.4, 100 mM NaCl, 1 mM EDTA, 1 mM EGTA, 1 mM NaF, 20 mM Na4P2O7, 2 mM Na3VO4, 0.1% sodium dodecylsulfate, 0.5% sodium deoxycholate, 1% Triton X-100, 10% glycerol, 10 mg/ml leupeptin, 60 mg/ml aprotinin, and 1 mM phenylmethanesulfonyl fluoride (PMSF). The extracted proteins were resolved by using either a 8% or 15% SDS-PAGE gel, followed by transfer to a polyvinylidene difluoride membrane (Bio-Rad) prior to immunoblotting.

Real-time PCR

Total RNA was isolated with use of TRIzol reagent (Invitrogen). Quantitative real-time PCR (qRT-PCR) with the TaqMan miRNA assay kit (Applied Biosystems) was used to measure the level of miR-33. The quantitative PCR (qPCR) was performed with an iQ SYBR Green Supermix (Bio-Rad) using iCycler Real-time PCR Detection System (Bio-Rad). The primer sequences are in the Supplemental Table section.

Primer Sequences Used in CHIP assay

Primers used for detection of the binding of SREBP2 to the three SREBP2 binding sites (SRE1, SRE2, SRE3) in the human NOX2 promoter were as follows: forward sequence (SRE1) 5'-TTGCCTGGAAACATGATTGCCA-3' , and the reverse sequence 5'-CCAGAGCAGTTCAGTTACTTGGCC-3', and forward sequence (SRE2) 5'-ACCAGCATTGCCACAAACACATGA-3', and the reverse sequence 5'-TCAGGAGGCTGAGGCAGGAGA-3', and forward sequence (SRE3) 5'-CTACAGGTGCCCACCACCATG-3', and the reverse sequence 5'-CTTTGGCCAATGATGAACCACATGT-3'. Primers used for detection of the binding of SREBP2 to the SREBP2 binding sites in the human NLRP3 promoter were as follows: forward sequence 5'-AAGATCCCAGGTTCAGCCAATGAGC-3', and the reverse sequence 5'-AGGTGCTGAAGCTAGAGAGAAAGCA-3'.

Measurement of ROS Production

After adenovirus infection, cells were exposed to 10 μM cell-permeable 2',7'-dichlorodihydrofluorescein diacetate (H2DCFDA) (Invitrogen), and ROS fluorescence

was measured with use of a Perkin Elmer Victor 2 1420 multi-label counter at 485-nm excitation and 535-nm emission. MitoSOX (Molecular Probes) was used as a live cell-permeable and mitochondrial localizing superoxide indicator. After adenovirus infection, cells were exposed to 2.5 μM MitoSOX for 30 min at 37 °C. Fluorescence intensity was measured using BD Biosciences FACSCanto II flow cytometer. For each analysis, 10,000 events were recorded. The data was analyzed using FCS Express analysis software (De Novo Software).

EC-SREBP2(N) Transgenic Mice

The SacI/BamHI fragment of HA-SREBP2(N) from pCMV5-HA-SREBP2(N) [2] was inserted into the EcoRV site of a pBluescriptIIKS vector containing an SV40 polyA signal. The SalI/XhoI fragment of the vascular endothelial-cadherin (VE-cadherin) promoter was then subcloned into the SalI site of the above-mentioned construct to yield pKSIICAD-BP2N2pA. The transgene was released by SalI/NotI double digestion followed by purification. Fertilized embryos from the hybrid strain CB6, an F1 hybrid between a BalbC and C57BL/6J mouse, were microinjected with the transgene at the UCSD transgenic mouse core facility. DNA from tails of the offspring was isolated and subjected to polymerase chain reaction (PCR). Mice with high levels of transgene incorporation were crossbred with C57BL/6J mice for two additional generations.

Vasodilatation Assay

The animal experimental protocols were approved by the Institutional Animal Care and Use Committee of University of California, Riverside. The middle cerebral arteries from

wild-type and EC-SREBP2(N)-Tg mice were isolated. For the flow-induced vasodilatation, the isolated mouse arteries were mounted on two glass cannulae in a perfusion myograph chamber connected to the SoftEdge Acquisition Subsystem (Living Systems, Burlington, VT). The vessel chamber was perfused with warmed physiological salt solution containing 130 mM NaCl, 10 mM HEPES, 6 mM glucose, 4 mM KCl, 4 mM $NaHCO_3$, 1.8 mM $CaCl_2$, 1.18 mM KH_2PO_4, 1.2 mM $MgSO_4$, and 0.025 mM EDTA, pH 7.4. Images of carotid arteries were obtained by a video camera attached to a Nikon TS100 inverted microscope. A video dimension analyzer (Living System) was used to measure the external diameter of arteries, and data were collected by use of BioPac MP100 hardware and Biopac AcqKnowledge software (BioPac, Goleta, CA). The arteries were maintained at an intraluminal pressure of 100 mmHg for the duration of each experiment, and then equilibrated for 30 min before extraluminal administration of 40-80 mM KCl (Sigma). After maximal constriction, flow, endothelium-dependent acetylcholine (ACh), and endothelium-independent sodium nitroprusside (SNP) vasodilating agents were applied. The vessel diameter changes were then recorded.

Endothelial Monocyte Adhesion Assay

Monocyte adhesion to HUVEC monolayers was determined by using a CytoSelect Adhesion Assay Kit (Cell Biolabs). HUVECs were transfected with control siRNA, NOX2 siRNA, or NLRP3 siRNA, then infected with Ad-SREBP2(N) or Ad-null for 24 hr. The infected cells were also treated with or without caspase-1 inhibitor Z-YVAD-FMK (2 μM) for 24 hr. THP1 monocytes (1×10^5 cells/well) were labeled with LeukoTracker and incubated for 30 min at 37 °C. To quantify monocyte adhesion, a Perkin Elmer Victor 2 1420

multi-label counter was used to measure fluorescence of lysed cells at 480-nm excitation and 520-nm emission.

Histology

The whole hearts were harvested, fixed in 4% paraformaldehyde in PBS overnight and, stepwise, dehydrated in 30%, 50%, 70%, 90% and 100% ethanol, each for 30 min. Tissues were subsequently incubated in xylene for 30 min at room temperature and embedded in paraffin at 55 °C. Five-μm cross sections were prepared and stained with Hematoxylin and eosin.

En face immunostaining

Mouse aortas were fixed and excised for determination of SREBP2, NOX2 and NLRP3 levels in the intima by en face immunostaining. Rabbit anti-SREBP2 (Abcam), mouse anti-NOX2 (BD Transduction Laboratory), and goat anti-NLRP3 (Abcam) were used as primary antibody at 1:100 dilution and incubated at 4 ºC overnight. Anti-rabbit TRITC, anti-mouse Alexa Fluor 488, and anti-goat FITC were used as secondary antibody. Slides were mounted with Prolong antifade reagent. Images were acquired using Leica TCS SP5 confocal microscope (Leica Microsystems, Wetzlar, Germany), with immersion lenses HC PL APO 20X / 0.75 IMM and pinhole [airy] 1.24.

Supplemental Table

Table S1. Real-time PCR Primer Sequences

Name	Species		Sequence
SREBP2	Homo sapiens	Forward	CCCTGGGAGACATCGACGA
		Reverse	CGTTGCACTGAAGGGTCCA
SREBP2	Mus musculus	Forward	GCGTTCTGGAGACCATGGA
		Reverse	ACAAAGTTGCTCTGAAAACAAATCA
SREBP1	Homo sapiens	Forward	ACTTCCCTGGCCTATTTGACC
		Reverse	GGCATGGACGGGTACATCTT
SREBP1	Mus musculus	Forward	GCAGCCACCATCTAGCCTG
		Reverse	CAGCAGTGAGTCTGCCTTGAT
HMG-CoA synthase	Homo sapiens	Forward	GGTCACGCTTGTGCCCGAAGGA
		Reverse	TGGCCAGCAAGCTTCTGCATTCA
HMG-CoA reductase	Homo sapiens	Forward	TGTTGGAGTGGCAGGACCCCTT
		Reverse	CTGGCACCTCCACCAAGACCTAT
Squalene synthase	Homo sapiens	Forward	CTGGTGCGCTTCCGGATCGG
		Reverse	ACTGCGTTGCGCATTTCCCC
LDLR	Homo sapiens	Forward	TCACCAAGCTCTGGGCGACG
		Reverse	GTAGCCGTCCTGGTTGTGGCA
IL-1β	Homo sapiens	Forward	AGGCACAAGGCACAACAGGCTG
		Reverse	GTCCTGGAAGGAGCACTTCATCTGT

IL-1β	Mus musculus	Forward	ATGAGAGCATCCAGCTTCAA
		Reverse	TGAAGGAAAAGAAGGTGCTC
Caspase 1	Homo sapiens	Forward	CTTCCTTTCCAGCTCCTCAGGCA
		Reverse	CGTGTGCGGCTTGACTTGTCC
Caspase 1	Mus musculus	Forward	AGGCATGCCGTGGAGAGAAACAA
		Reverse	AGCCCCTGACAGGATGTCTCCA
ASC	Homo sapiens	Forward	CAGCCAAGCCAGGCCTGCACTTTAT
		Reverse	GCAGGTCCAGTTCCAGGCTGGT
ASC	Mus musculus	Forward	AGACATGGGCTTACAGGA
		Reverse	CTCCCTCATCTTGTCTTGG
NLRP1	Homo sapiens	Forward	CCAGCCCGCATAGCCGTACC
		Reverse	CCGGTCCCAGGACTGGCTCA
NLRP1a	Mus musculus	Forward	AGGCTCTTTACCCTCTTCTA
		Reverse	ATGTGCTTCTTCTTCTGGTA
NLRP1c	Mus musculus	Forward	GAATCTTTACTCCACCCAGC
		Reverse	CTTTTCCTGGCAAATGTCTT
NLRP3	Homo sapiens	Forward	TGCCGGGGCCTCTTTTCAGT
		Reverse	CCACAGCGCCCCAACCACAA
NLRP3	Mus musculus	Forward	TGTGAGAAGCAGGTTCTACTCT
		Reverse	GACTGTTGAGGTCCACACTCT
NOX1	Homo	Forward	CTGCTTCCTGTGTGTCGCAA

	sapiens	Reverse	AGGCAGATCATATAGGCCACC
NOX1	Mus	Forward	GGTTGGGGCTGAACATTTTTC
	musculus	Reverse	TCGACACACAGGAATCAGGAT
NOX2	Homo	Forward	AACGAATTGTACGTGGGCAGA
	sapiens	Reverse	GAGGGTTTCCAGCAAACTGAG
NOX2	Mus	Forward	GGCTGGGATGAATCTCAGGCCAA
	musculus	Reverse	ACTGGTTTCCTGGTGAAAGAGCGG
NOX4	Homo	Forward	ACCCGGCTCTGGGTAGCAGAC
	sapiens	Reverse	AGAGCCAGATGAACAGGCAGAGGT
NOX4	Mus	Forward	GTCCTGAGCACCGAGCAGGG
	musculus	Reverse	GGGACAGCCAAATGAGCAGGCA
p22phox	Homo	Forward	CCCAGTGGTACTTTGGTGCC
	sapiens	Reverse	GCGGTCATGTACTTCTGTCCC
p22phox	Mus	Forward	GTGTGATCTATCTGCTGGCAGCCA
	musculus	Reverse	GCCTCCTCTTCACCCTCACTCGG
p40phox	Homo	Forward	TTGACCGCATGGCAGCTCCG
	sapiens	Reverse	ACCGCGATGTCCTTGATGGTGC
p40phox	Mus	Forward	AGGGCGGGACCTCCTCAAAGG
	musculus	Reverse	GCTGCTCAAAGTCGCTCTCTGATCG
p47phox	Homo	Forward	CGTACCGCGCCATTGCCAAC
	sapiens	Reverse	GAACCACCAACCGCTCTCGCT

p47phox	Mus musculus	Forward	TGGCACAAAGGACAATCCATCGAC
		Reverse	GGGATAGGAGCCGTCTAGGGCC
p67phox	Homo sapiens	Forward	CCCACTCCCGGATTTGCTTC
		Reverse	GTCTCGGTTAATGCTTCTGGTAA
p67phox	Mus musculus	Forward	ACCTTGAAGCCTGGAGCGCCTA
		Reverse	GATGCTTTTGGTGAAGGCCTGCTCG
MCP-1	Homo sapiens	Forward	CGCTCAGCCAGATGCAATCAATGC
		Reverse	GGTTTGCTTGTCCAGGTGGTCCA
MCP-1	Mus musculus	Forward	TTAAAAACCTGGATCGGAACCAA
		Reverse	GCATTAGCTTCAGATTTACGGGT
VCAM-1	Homo sapiens	Forward	TGTCAATGTTGCCCCCAGAGATACA
		Reverse	GGCTGTAGCTCCCCGTTAGGGA
VCAM-1	Mus musculus	Forward	AGTTGGGGATTCGGTTGTTCT
		Reverse	CCCCTCATTCCTTACCACCC
ICAM-1	Homo sapiens	Forward	GTGTCCTGTATGGCCCCCGACT
		Reverse	ACCTTGCGGGTGACCTCCCC
ICAM-1	Mus musculus	Forward	GCTACCATCACCGTGTATTCG
		Reverse	TAGCCAGCACCGTGAATGTG
E-selectin	Homo sapiens	Forward	GTGACATGCAGGGCCGTCCG
		Reverse	AGGCTGTGCACTGGAAAGCTTCA
E-selectin	Mus	Forward	CCAATCTGAAACATTCACCGAGT

	musculus	Reverse	CGAGTCTTTGGTTCGTTGGATG
β-actin	Homo	Forward	CATGTACGTTGCTATCCAGGC
	sapiens	Reverse	CTCCTTAATGTCACGCACGAT
GAPDH	Mus	Forward	AGGCCGGTGCTGAGTATGTC
	musculus	Reverse	TGCCTGCTTCACCACCTTCT

Figure. S1

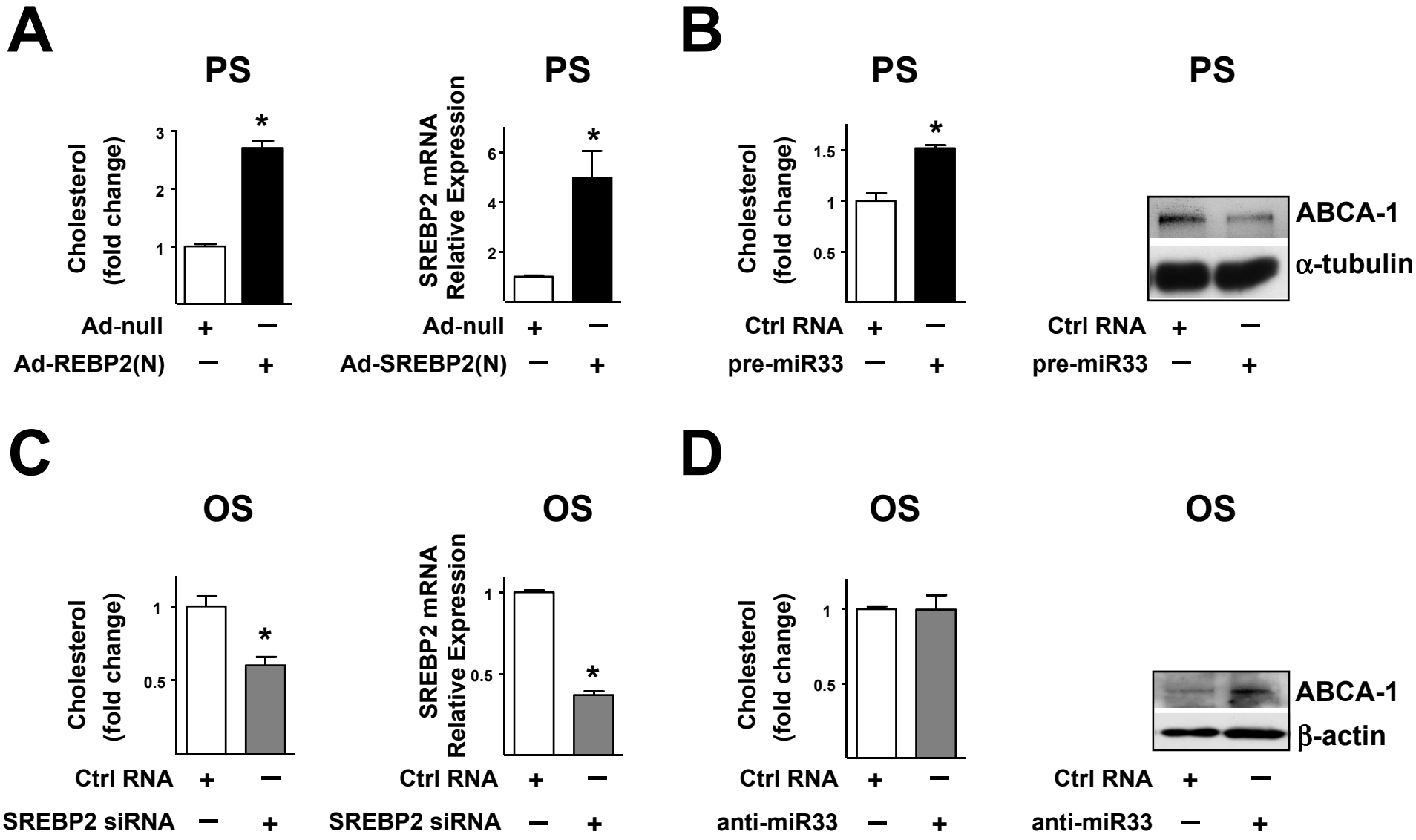
A
PS
Cholesterol (fold change)
3
2
1
*
Ad-null + −
Ad-REBP2(N) − +
PS
SREBP2 mRNA Relative Expression
6
4
2
*
Ad-null + −
Ad-SREBP2(N) − +
B
PS
Cholesterol (fold change)
1.5
1
0.5
*
Ctrl RNA + −
pre-miR33 − +
PS
ABCA-1
α-tubulin
Ctrl RNA + −
pre-miR33 − +
C
OS
Cholesterol (fold change)
1
0.5
*
Ctrl RNA + −
SREBP2 siRNA − +
OS
SREBP2 mRNA Relative Expression
1
0.5
*
Ctrl RNA + −
SREBP2 siRNA − +
D
OS
Cholesterol (fold change)
1
0.5
Ctrl RNA + −
anti-miR33 − +
OS
ABCA-1
β-actin
Ctrl RNA + −
anti-miR33 − +

Figure. S2

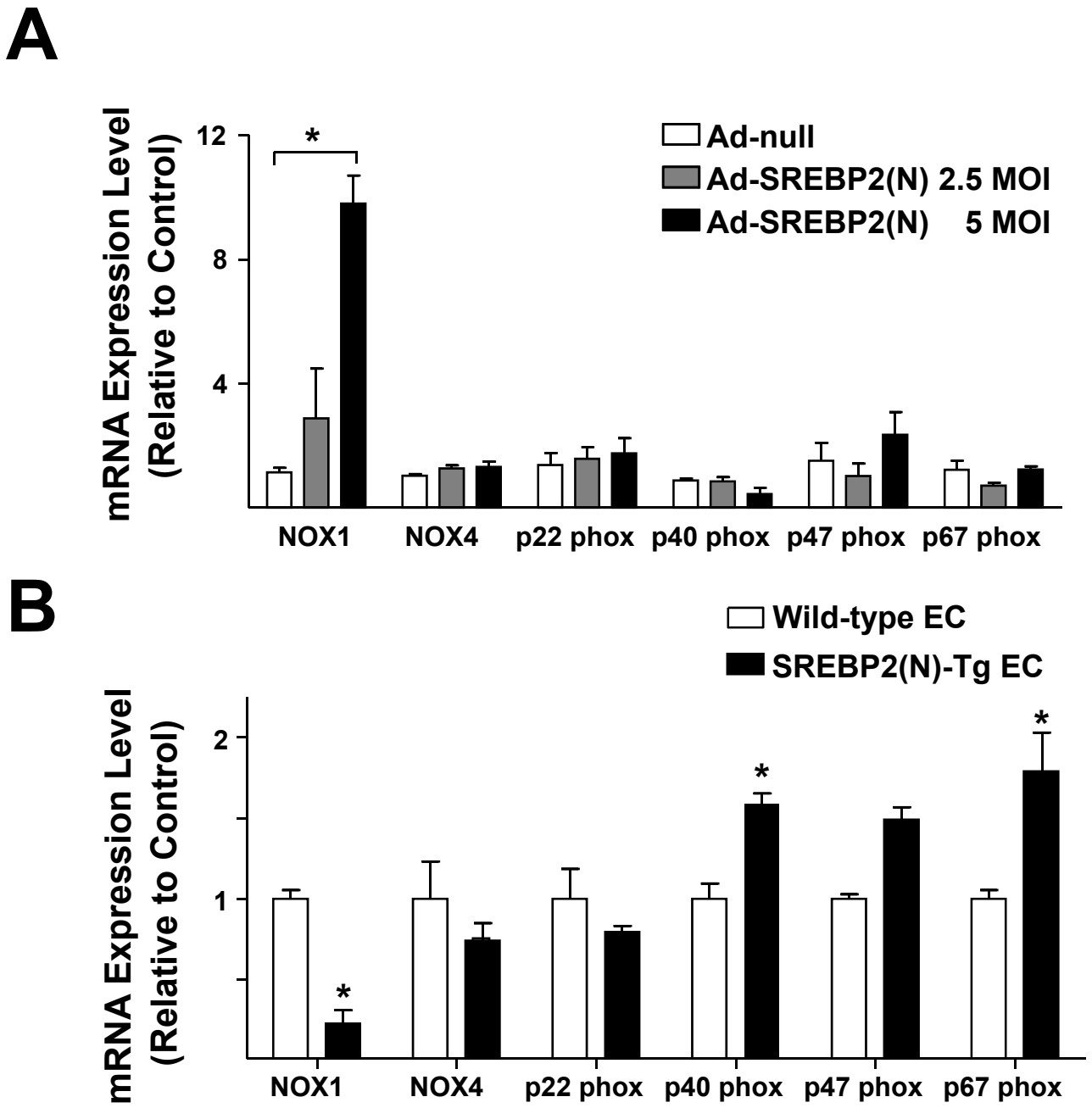
A
mRNA Expression Level
(Relative to Control)
12
8
4
*
Ad-null
Ad-SREBP2(N) 2.5 MOI
Ad-SREBP2(N) 5 MOI
NOX1
NOX4
p22 phox
p40 phox
p47 phox
p67 phox
B
Wild-type EC
SREBP2(N)-Tg EC
mRNA Expression Level
(Relative to Control)
2
1
*
*
*
NOX1
NOX4
p22 phox
p40 phox
p47 phox
p67 phox

Figure. S3

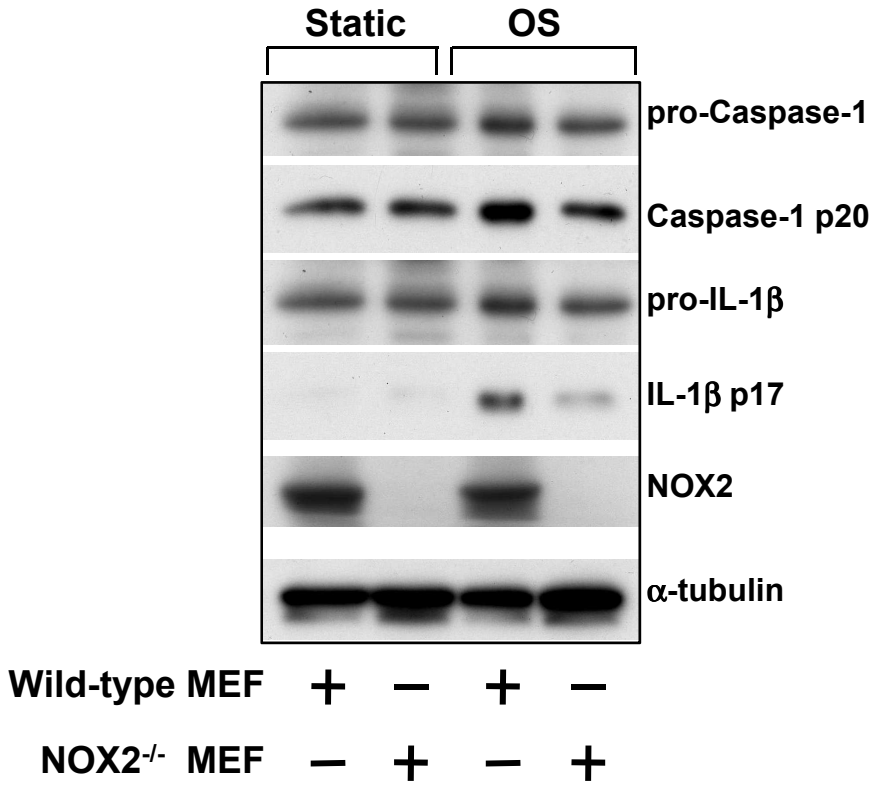
Static
OS
pro-Caspase-1
Caspase-1 p20
pro-IL-1β
IL-1β p17
NOX2
α-tubulin
Wild-type MEF + − + −
NOX2-/- MEF − + − +

Figure. S4

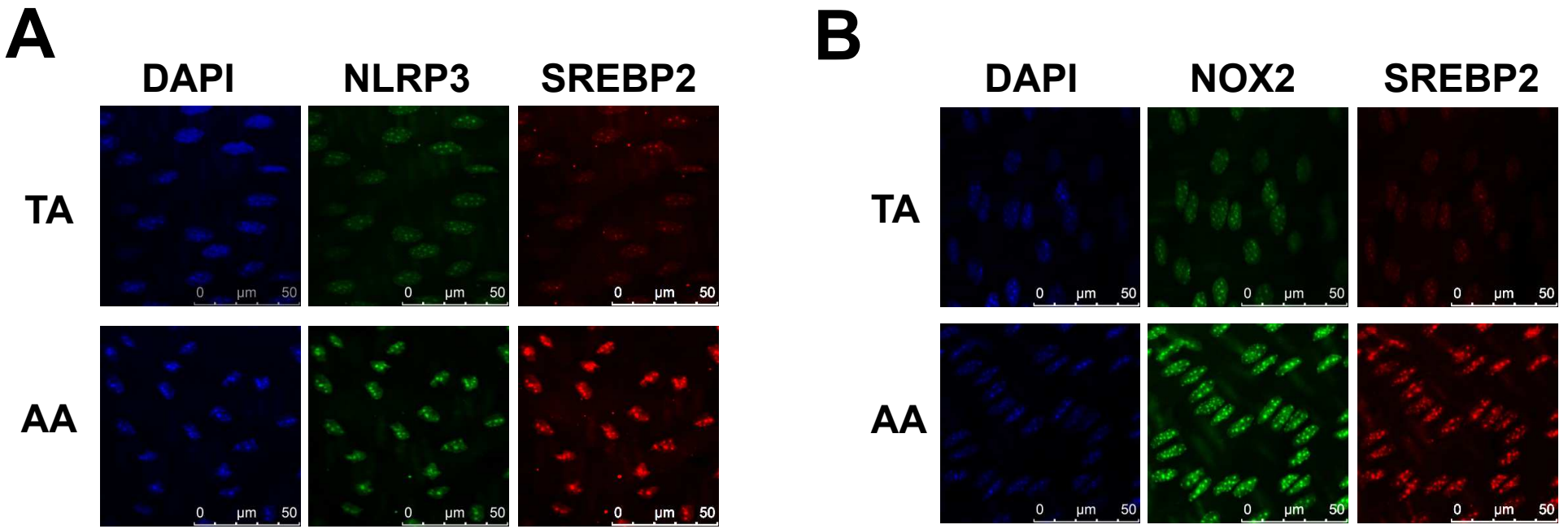

Figure. S5

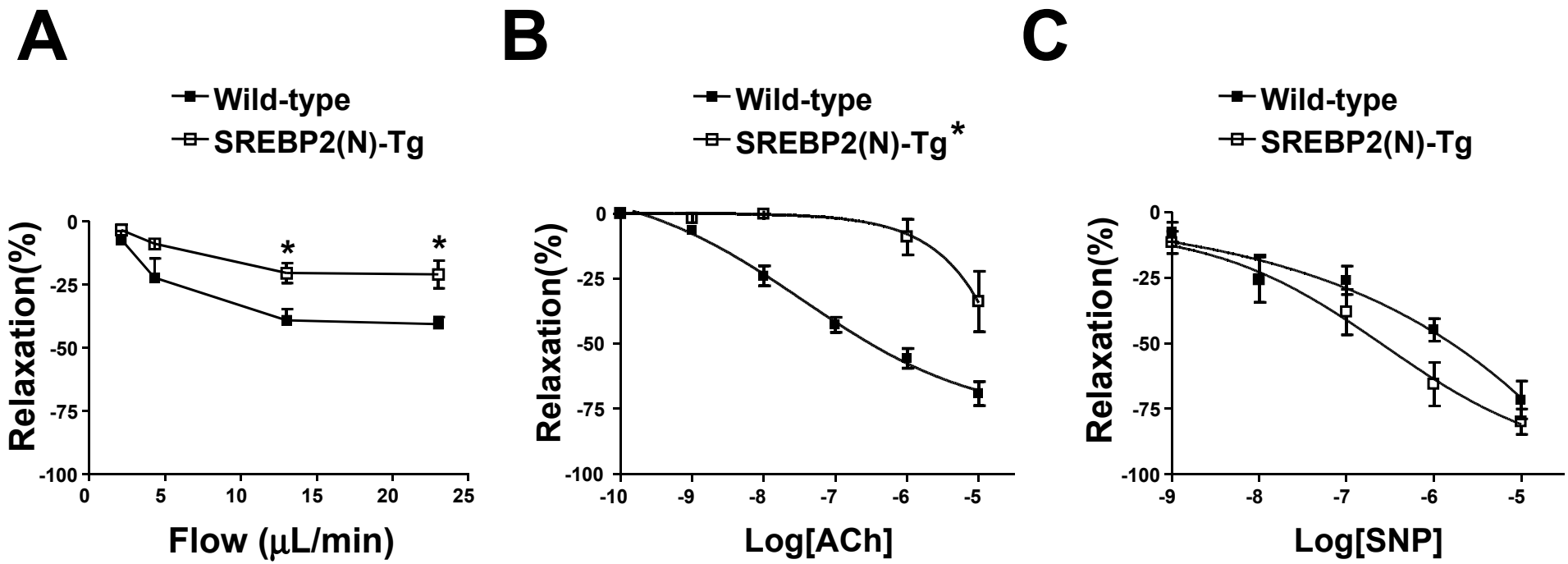
A
Wild-type
SREBP2(N)-Tg
Relaxation(%)
0
-25
-50
-75
-100
0
5
10
15
20
25
*
*
Flow (μL/min)
B
Wild-type
SREBP2(N)-Tg*
Relaxation(%)
0
-25
-50
-75
-100
-10
-9
-8
-7
-6
-5
Log[ACh]
C
Wild-type
SREBP2(N)-Tg
Relaxation(%)
0
-25
-50
-75
-100
-9
-8
-7
-6
-5
Log[SNP]

Figure. S6

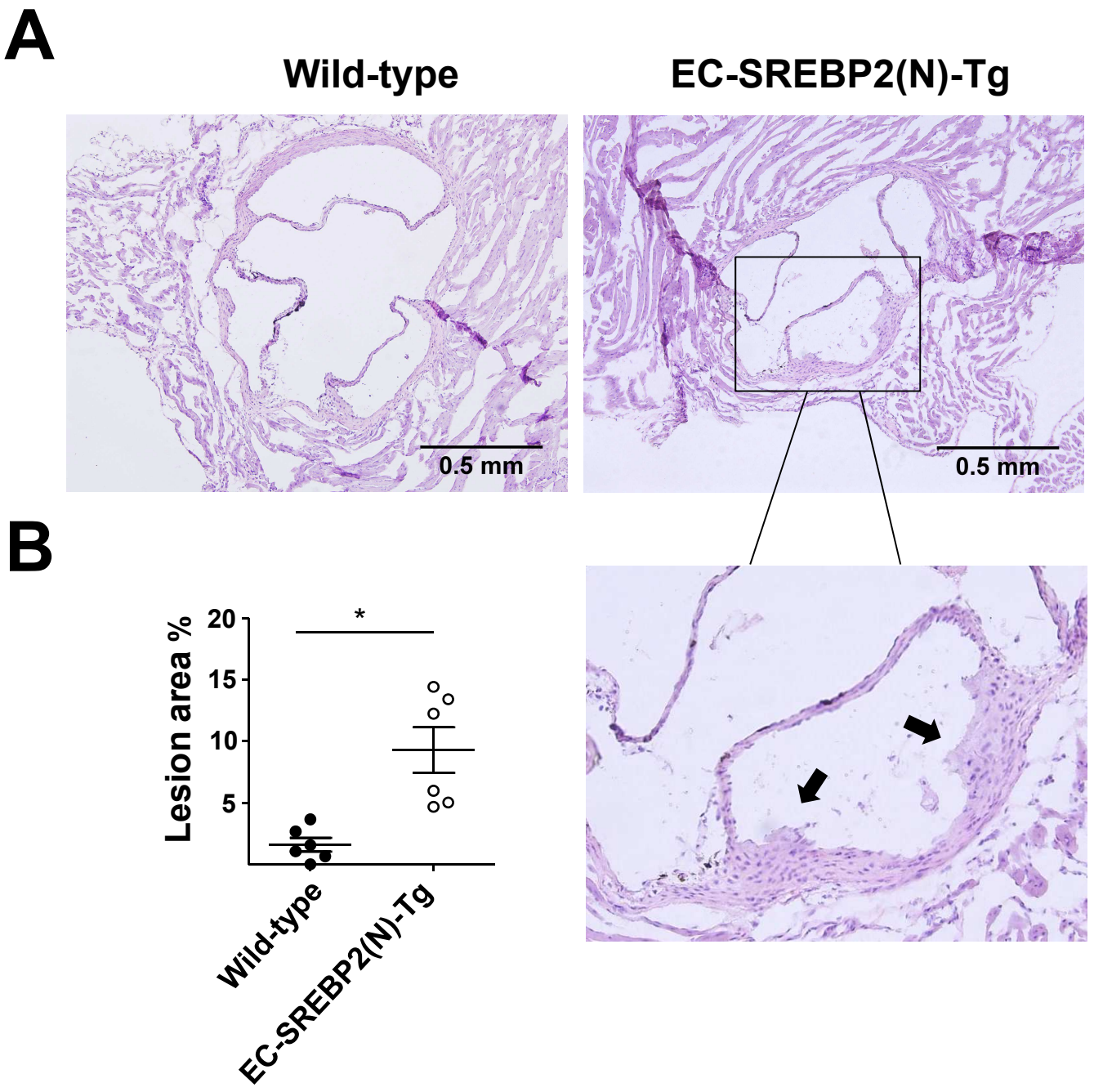
A
Wild-type
EC-SREBP2(N)-Tg
0.5 mm
0.5 mm
B
Lesion area %
20
15
10
5
*
Wild-type
EC-SREBP2(N)-Tg

Figure. S7

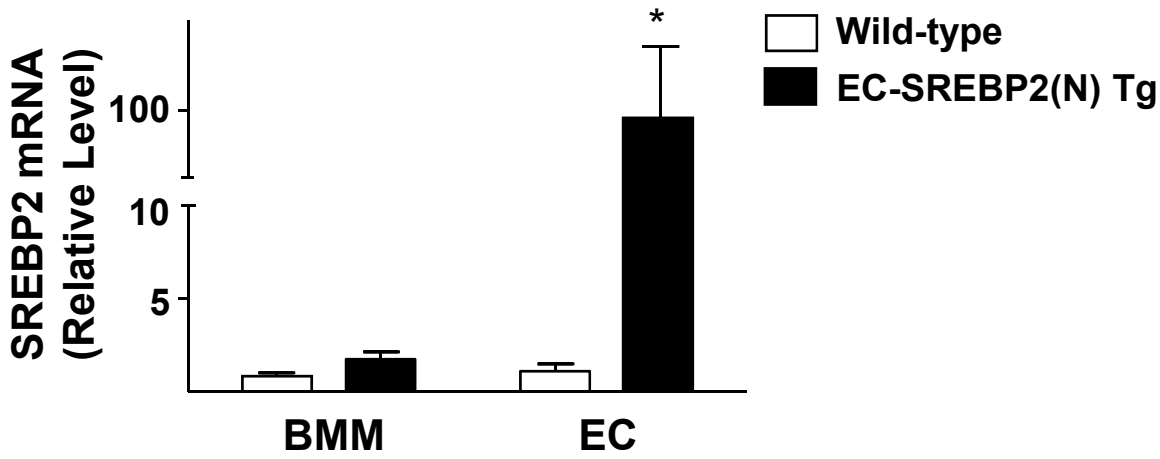
SREBP2 mRNA
(Relative Level)
100
10
5
*
BMM
EC
Wild-type
EC-SREBP2(N) Tg

Figure. S8

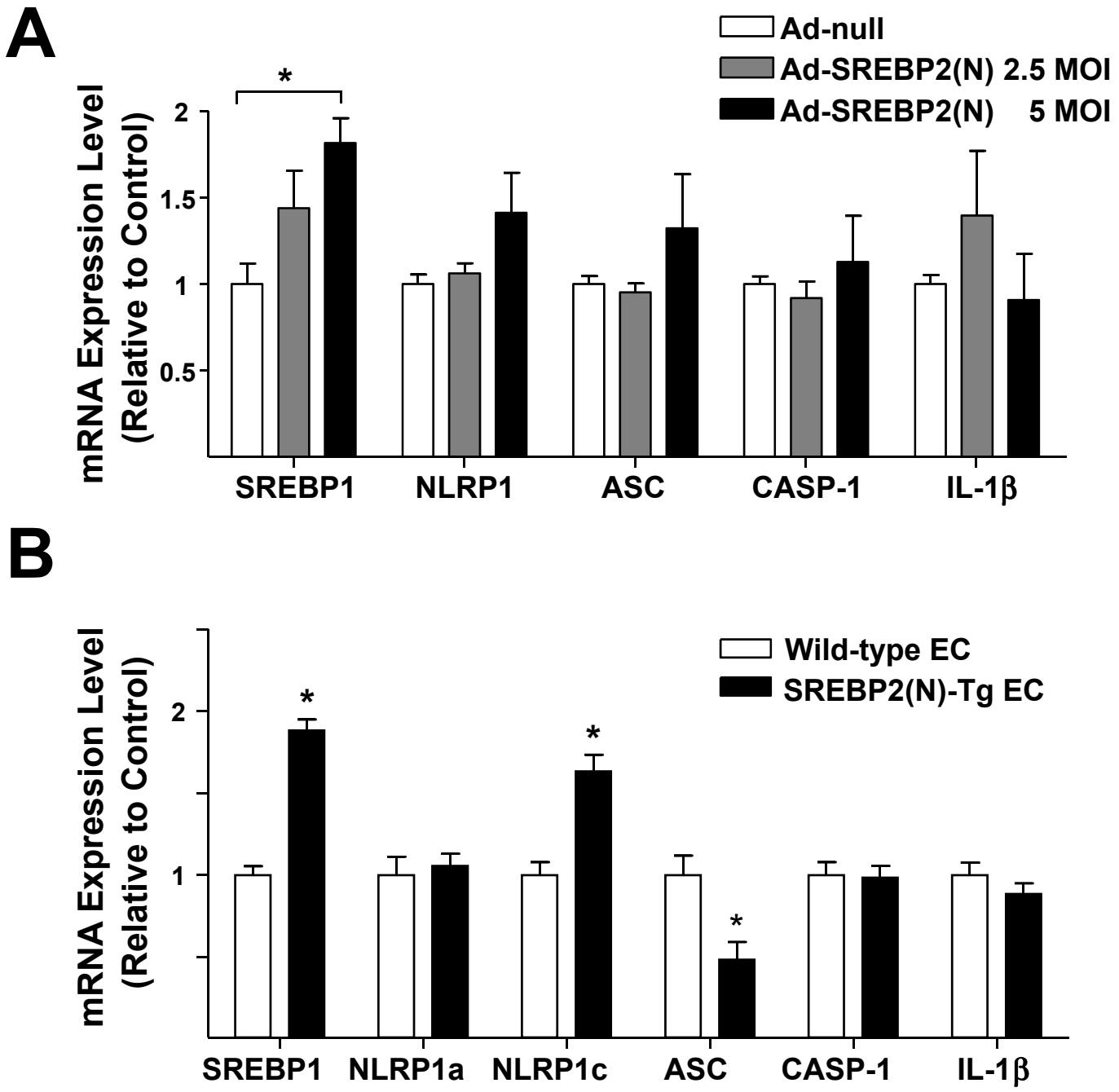
A
Ad-null
Ad-SREBP2(N) 2.5 MOI
Ad-SREBP2(N) 5 MOI
mRNA Expression Level
(Relative to Control)
2
1.5
1
0.5
*
SREBP1
NLRP1
ASC
CASP-1
IL-1β
B
Wild-type EC
SREBP2(N)-Tg EC
mRNA Expression Level
(Relative to Control)
2
1
*
*
*
SREBP1
NLRP1a
NLRP1c
ASC
CASP-1
IL-1β

Supplemental figure legends

Figure S1. SREBP2, but not miR-33, Is Required for OS-induced Cholesterol Accumulation in HUVECs. (A) Cholesterol and SREBP2 mRNA levels in cells infected with Ad-null or Ad-SREBP2(N) (2.5 MOI) and then exposed to PS. (B) Cholesterol and ABCA-1 levels in cells treated with control RNA or pre-miR33 (30 nM) and then exposed to PS. (C) Cholesterol and SREBP2 mRNA levels in cells transfected with 20 nM control RNA or SREBP2 siRNA and exposed to OS. (D) Cholesterol and ABCA-1 levels in cells transfected with control RNA or anti-miR33 (20 nM) and exposed to OS. The duration for PS and OS was 14 hr. Experiments were performed in triplicate and data are expressed as means ± SEM. Statistical significance was evaluated by using Mann-Whitney U test with exact method, where $p < 0.05$ is indicated by '*'.

Figure S2. SREBP2 Induces NOX Subunits in ECs. mRNA levels of NOX1, NOX4, p22 phox, p40 phox, p47 phox and p67 phox in (**A**) HUVECs infected with Ad-null (2.5 MOI) or Ad-SREBP2(N) (2.5 MOI and 5 MOI) and (**B**) lung ECs isolated from the wild-type or SREBP2(N)-Tg mice (n = 8/group). Experiments were performed in triplicate and data are expressed as mean ± SEM. Statistical significance was evaluated by using Mann-Whitney U test with exact method, where '*' indicates $p < 0.05$.

Figure S3. OS-induced inflammasome is attenuated in NOX2$^{-/-}$ mouse embryonic fibroblasts (MEFs). Representative immunoblot of pro-caspase-1, caspase-1 p20, pro-IL-1β, IL-1β p17, and NOX2 in the wild-type and NOX2$^{-/-}$ MEFs under static conditions or OS for 14 hr.

Figure S4 Elevated level of SREBP2, NOX2, and NLRP3 in the endothelium of the mouse aortic arch. Representative images of SREBP2 (red), NLRP3 (green), and nucleus (blue) in (A) and SREBP2 (red), NOX2 (green), and nucleus (blue) in (B) from thoracic aorta (TA) and aortic arch (AA) of C57/BL6 mice.

Figure S5. Overexpression of EC-SREBP2(N) Impairs the Endothelial-dependent Vascular Tone. The vasorelaxation responses of isolated middle cerebral arteries from EC-SREBP2(N)-Tg mice and their wild-type littermates were compared with respect to vasodilatation induced by flow (**A**), acetylcholine (ACh) (**B**), or sodium nitroprusside (SNP) (**C**). The results are presented as mean ± SEM. Statistical significance is evaluated by using two-way ANOVA analysis with Bonferroni post-hoc test (**A**) or *F* test of Log(EC_{50}) (**B&C**), where $p < 0.05$ is indicated by '*'. The results show that the vasodilation responding to flow and ACh, but not SNP, is impaired.

Figure S6. Early Atherosclerotic Lesions Develop in The Aortic Roots of EC-SREBP2(N)-Tg Mice. Histological sections stained with H&E of aortic roots from (**A**) male EC-SREBP2(N)-Tg mice (n = 6) and their wild-type littermates (n = 6) fed an atherogenic diet for 20 weeks and then were killed. Atherosclerotic lesions are indicated with an arrow. (**B**) Quantification of the percentage of lesion area for the wild-type mice and EC-SREBP2(N)-Tg mice. Statistical significance was evaluated by using Student's *t* test, where $p < 0.05$ is indicated by '*'.

Figure S7. Low Expression of SREBP2(N) Transgene in The Bone Marrow Macrophages of EC-SREBP2(N)-Tg Mice. mRNAs were collected from bone marrow

macrophages (BMM) and EC of the wild-type littermates (n = 5) and EC-SREBP2(N)-Tg mice (n = 5). The level of SREBP2 mRNA was determined by RT-PCR with the use of primers for the transgene. Statistical significance was evaluated by using Mann-Whitney U test with exact method, where $p < 0.05$ is indicated by '*'

Figure S8. SREBP2(N) Overexpression Induces SREBP1 and NLRP1c in ECs. mRNA levels of SREBP1, NLRP1a，NLRP1c, ASC, caspase-1 and IL-1β in (**A**) HUVECs infected with Ad-null (2.5 MOI) or Ad-SREBP2(N) (5 MOI) or in (**B**) lung ECs isolated from the wild-type or SREBP2(N)-Tg mice (n = 8/group). Experiments were performed in triplicates and data are expressed as mean ± SEM. Statistical significance was evaluated by using Mann-Whitney U test with exact method, where $p < 0.05$ is indicated by '*'.

Supplemental References

1. Lim YC, Luscinskas FW. Isolation and culture of murine heart and lung endothelial cells for in vitro model systems. *Methods. Mol. Biol.* 2006;341:141-154.

2. Lin T, Zeng L, Liu Y, DeFea K, Schwartz MA, Chien S, Shyy JY. Rho-ROCK-LIMK-cofilin pathway regulates shear stress activation of sterol regulatory element binding proteins. *Circ. Res.* 2003;92:1296-1304.